

Stability and efficiency issues, solutions and advancements in perovskite solar cells: A review

Ritika Sharma^a, Arushi Sharma^a, Shikha Agarwal^b, M.S. Dhaka^{a,*}

^a Department of Physics, Mohanlal Sukhadia University, Udaipur 313001 India

^b Department of Chemistry, Mohanlal Sukhadia University, Udaipur 313001 India



ARTICLE INFO

Keywords:

Photovoltaics
Perovskite solar cells
Fabrication techniques
Power conversion efficiency
Stability
Degradation

ABSTRACT

The modern era of cutting-edge technology needs alternative renewable energy resources due to limited stocks and pollution concerns dealing with the conventional resources. Solar photovoltaics (PV) has been recognized as one of the potential alternatives with environmental and cost-effective aspects. The conventional Silicon solar cells have been champion at both the laboratory and industrial scales and dominated the PV market owing to inexpensive generation of electricity, but its cost is relatively higher vis-à-vis to the second and third generation solar cell technologies. Over the years, the perovskite solar cells (PSCs) have grabbed incredible attention and attained excellent PV performance owing to their competitive power conversion efficiency (PCE) which hiked from 3.1 % to 25.7 % and could be a reasonable cost-effective alternative to Si-based technology too. Despite of the plagued performance and desirable properties of perovskite solar cells (PSCs), still these cells have stability issues and the maximum lifetime that a PSC attained is 1 year while the champion Silicon solar cells have a lifetime of up to 25 years. Therefore, to address the stability and efficiency issues, the present review deals with an evolution to the device architecture, electron transport, hole transport and perovskite absorber layers to the PSCs in terms of PCE and stability. Also, the chemical nature, properties, stability issues along with the commercialization grade and future insights to the PSCs have been portrayed.

1. Introduction

Limited stocks and environmental issues to the conventional energy resources invited attention so far to seek alternative energy resources for the future world. Among various available alternatives, solar energy is believed to be one of the most useful renewable energy resources as one hour of continuous illumination of sunlight can fulfill the annual power requirements of the world (Roy et al., 2020). In 1839, Edmund Becquerel discovered the photovoltaic (PV) effect and converted the sunlight into electricity (Becquerel and Acad, 1839). The photoconductivity in Selenium was discovered by Willoughby Smith in 1873 (Smith, 1873) and later in 1883, Charles Fritts introduced the first PV cell based on Selenium wafers (Fritts, 1883). In 1905, Albert Einstein explained the theory of light for ejection of electrons from the metal surface in terms of photoelectric effect (Einstein, 1905). In 1918, Jan Czochralski laid the foundation for the Silicon based solar cells by discovering a technique based on the growth of single-crystal Silicon (Czochralski, 1918). In 1954, the first crystalline Silicon based solar cell was reported in Bell laboratories having an efficiency of 6 % (Nelson, 2002). In 1990s, the

developed countries have started to release grants for the development of solar cells (Nelson, 2002). Meanwhile, the second-generation and third-generation solar cells have come into existence and during 2009, the first ever PSCs were developed having a PCE of 3.1 % (Kojima et al., 2009) and to the date, the power conversion efficiency of the PSCs have reached 25.7 % for the single junction devices (NREL Best Research-Cell Efficiency Chart, 2022). In order to develop cost effective solar cell technology, three generations of solar cells come into existence where persistent efforts have been made so far to demonstrate cost effective, stable and efficient devices. Based upon the available literature, development history of the solar cells is briefly depicted in Fig. 1.

Although the first generation conventional Silicon solar cells dominate the PV market owing to their inexpensive electricity generation yet due to its relatively higher cost vis-à-vis to the others, researchers are seeking for new PV technology that should not only cost effective but provide higher PCE too (Nelson, 2002; "The History of Solar Energy", 2013; Green et al., 2018). The second generation is thin film based while the perovskite solar cells are also thin film based and categorized under third generation those have accomplished colossal recognition due to

* Corresponding author.

E-mail addresses: msdhaka75@yahoo.co.in, msdhaka@mlsu.ac.in (M.S. Dhaka).

their desirable properties, improved stability and PCE.

The perovskites are basically a class of compounds having ABX_3 configuration and a pictorial view is depicted in Fig. 2 comprising of locations to the atoms of its different constituents.

The perovskite solar cells have gained massive popularity and recognized as potential alternative to the champion Silicon solar cells due to their ease of fabrication, low-cost, high absorption coefficient, controllable band gap, high charge carrier mobility etc. (Roy et al., 2020; Nair et al., 2020) provided to resolve stability and degradation issues followed by commercialization. To the date, the PCE of PSCs has been reached from 3.1 % to 25.7 % for the single junction and to 31.3 % for the tandem architecture (Kojima et al., 2009; NREL Best Research-Cell Efficiency Chart, 2022; Wu et al., 2021). The perovskite solar cells developed employing chemical route based solution processes have demonstrated decent PCE with cost effectiveness (Mai et al., 2022) and consequently, these have been recognized as rivalry to the champion Silicon solar cells. The chemical processes are cheaper as compared to the physical ones while the physical routes could provide better stability to the devices. The PSCs have outstanding commercialization potential those could create milestones but, there are so many factors those need to be solved. Some of the major factors those affect the performance of the PSCs are high cost of Gold electrodes, temperature, additives, degradation in presence of Oxygen, moisture and UV illumination, toxicity of Lead, thermal stress, electric biasing, interface etc (Sutton et al., 2016; Cao et al., 2022; Leguy et al., 2015; Wali et al., 2020). Also to the date, the maximum lifetime attained by perovskite solar cells is just a year while it is about 25 years for the Silicon solar cells. The shorter lifetime is a major obstacle for the PSCs to their commercialization as the IEC 61215 test protocols need that pre-requisites for stable devices should have lesser than 10 % drop in PCE for 1000 hrs duration with lifetime warranty of 20–25 years (Manor et al., 2011; Wang et al., 2016a; Berhe et al., 2016).

Although persistent efforts have been made so far to address these issues employing varying fabrication techniques, novel materials, Lead free inorganic compounds, interface engineering, doping and device architecture evolution to the perovskite solar cells yet these devices are weighed down by the same which ultimately affect the performance and stability. In light of the above, the present review focuses on current scenario regarding the stability and performance to the perovskite solar cells. It mainly includes historical background, properties, chemical nature, device architecture, development routes, factors dealing with reduction in stability and performance and commercialization strategy with further recommendations.

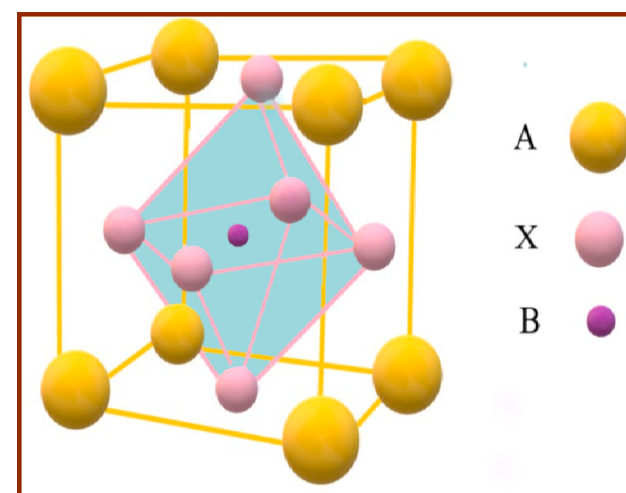


Fig. 2. A typical illustration of ABX_3 configuration to the perovskites comprising of constituent atoms positions in unit cell with cubic phase.

2. History of perovskite solar cells

2.1. Single junction perovskite solar cells

In this section, the development history of perovskite material ever since its invention in 1839 is depicted and then perovskite solar cell device demonstration in 2009 followed by attaining the augmented power conversion efficiencies in the successive years (Kojima et al., 2009; NREL Best Research-Cell Efficiency Chart, 2022; Katz, 2020; Rose, 1839; Mitzi et al., 2001; Im et al., 2011; Kim et al., 2012; Burschka et al., 2013; Im et al., 2014; Giordano et al., 2016; Yang et al., 2015; Li et al., 2016; Bi et al., 2016; Yang et al., 2017; Yang et al., 2018; Jiang et al., 2019; Green et al., 2020; Green et al., 2021) which is also summarized briefly by a pictorial representation in Fig. 3 and tabulated in Table 1 along with desired description.

In 1839, a mineral, CaTiO_3 was discovered in the Ural Mountains located in Russia followed by transporting the original mineral sample from Saint Petersburg to Berlin by a Russian mineralogist Alexander Kämmerer for further examination to a German mineralogist and crystallographer, Gustav Rose who analyzed it and determined chemical composition along with properties. Later, Kämmerer suggested Rose to recognize this mineral in name of Russian mineralogist Count Lev

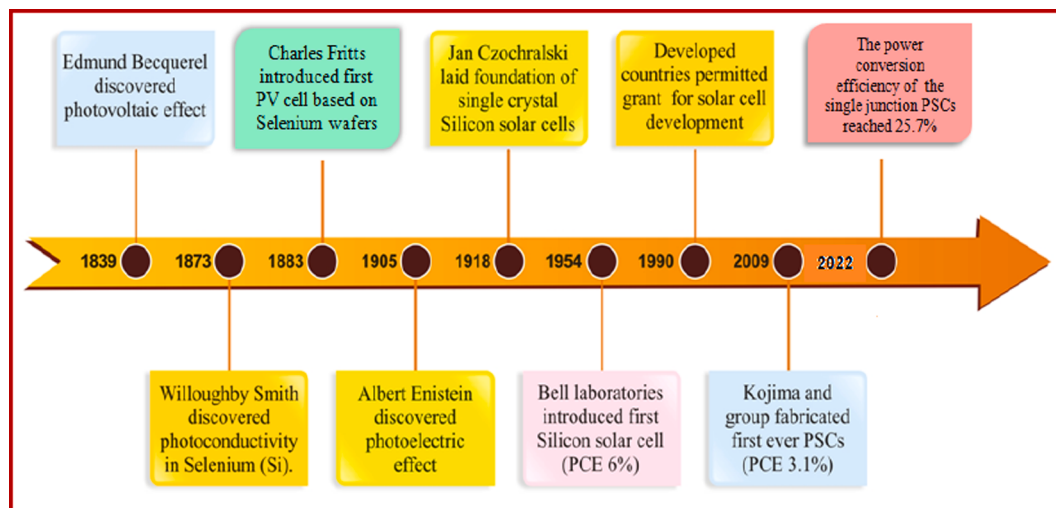


Fig. 1. Schematic representation of development history to the solar cells where the data are taken from references (Becquerel and Acad, 1839; Smith, 1873; Fritts, 1883; Einstein, 1905; Czochralski, 1918; Nelson, 2002; Kojima et al., 2009; NREL Best Research-Cell Efficiency Chart, 2022).

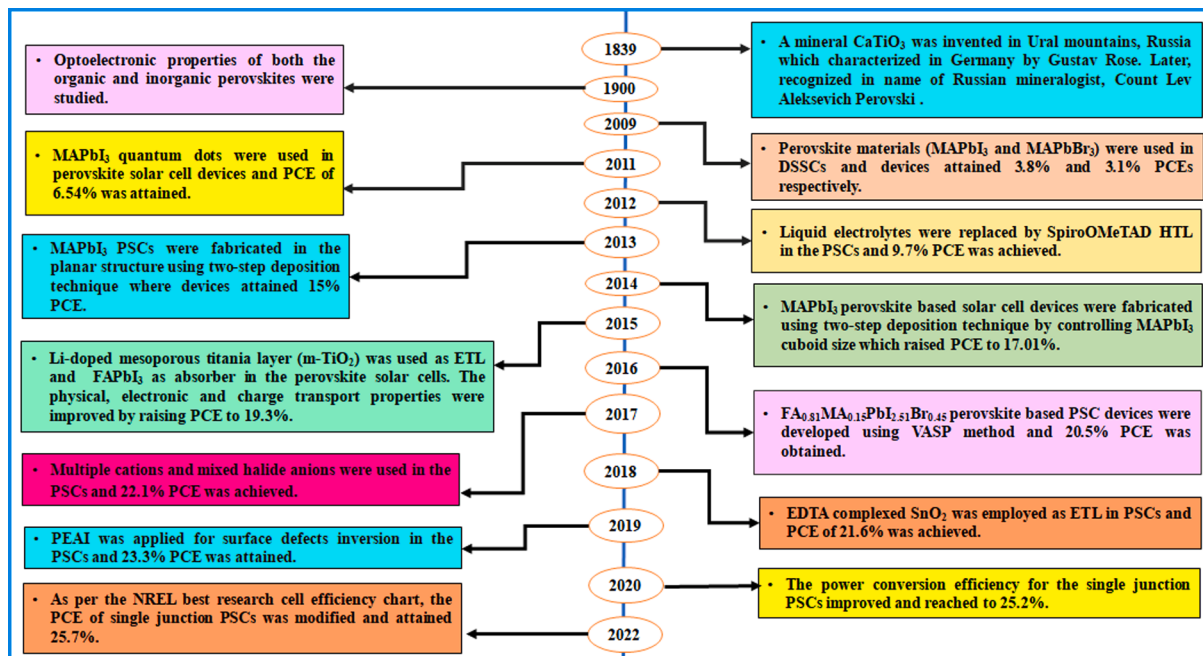


Fig. 3. A schematic representation of development history to the PSCs where data are taken from the references (Kojima et al., 2009; NREL Best Research-Cell Efficiency Chart, 2022; Katz, 2020; Rose, 1839; Mitzi et al., 2001; Im et al., 2011; Kim et al., 2012; Burschka et al., 2013; Im et al., 2014; Giordano et al., 2016; Yang et al., 2015; Li et al., 2016; Bi et al., 2016; Yang et al., 2017; Yang et al., 2018; Jiang et al., 2019; Green et al., 2020; Green et al., 2021).

Aleksevich Perovski who was a Politician too (Katz, 2020; Rose, 1839) and accordingly; this mineral was recognized as perovskite. In due course of time, the popular structure for the perovskite was ABX_3 and workers evolved the constituent atoms as per need of the technology.

In 1990s, researchers (Mitzi et al., 2001) studied the optoelectronic properties of both the organic and inorganic perovskites and found that these have desirable features which could be of immense use in the field of solar cells. In 2009, Kojima and others (Kojima et al., 2009) became the first ones to use the perovskite material as liquid sensitizer in the dye sensitized solar cells (DSSCs). They used $\text{CH}_3\text{NH}_3\text{PbI}_3/\text{MAPbI}_3$ and $\text{CH}_3\text{NH}_3\text{PbBr}_3/\text{MAPbBr}_3$ as liquid sensitizers and achieved efficiency of 3.8 % and 3.1 %, respectively but, these devices were highly unstable because of applying the liquid electrolyte. In 2011, the MAPbI_3 quantum dots were used and the PSC efficiency was raised from 3.81 % to 6.54 % while the device lasted only for 10 min due to the dissolution of quantum dots in redox electrolyte solution. The liquid electrolytes caused instabilities in the devices and needed to be overcome (Im et al., 2011). In 2012, the problem of the liquid electrolytes was solved by incorporating SpiroOMeTAD as HTL in the PSC device concerned where, the device achieved PCE of 9.7 %. It was considered as a breakthrough in the history of solar cells, since this device was demonstrated not only with increased efficiency but enhanced lifetime by 500 h too (Kim et al., 2012). In 2013, PSC was fabricated in a planar architecture where the PbI_2 layer was followed by $\text{CH}_3\text{NH}_3\text{I}$. This planar structure provided power conversion efficiency of 15 % (Burschka et al., 2013). The MAPbI_3 based solar cells were fabricated (Im et al., 2014) where cuboid size of the MAPbI_3 was controlled which led to enhanced light harvesting, improved charge transportation and as a consequence, power conversion efficiency reached to 17.01 %.

In 2015, the use of Li-doped mesoporous titania layer (m-TiO_2) was reported (Giordano et al., 2016) where, the electronic properties of the TiO_2 layers were studied and by doping of Lithium, the PCE of 19.3 % was achieved. Yang and coworkers (Yang et al., 2015) have used FAPbI_3 absorber layer in place of MAPbI_3 and observed that replacing Methylammonium (MA) by Formamidinium (FA) provided higher PCE of 20.1 % under AM1.5G full sun illumination. The $\text{FA}_{0.81}\text{MA}_{0.15}\text{PbI}_{2.51}\text{Br}_{0.45}$ absorber layer based perovskite solar cell devices were developed using

vacuum flash-assisted solution processing method (VASP) by Li and others (Li et al., 2016). The absorber layers have even morphology with crystalline behavior and devices concerned attained maximum PCE of 20.5 %. In 2016, a novel approach was employed (Bi et al., 2016) by using a polymer named poly (methylmethacrylate) (PMMA) for the fabrication of perovskite solar cell devices where electronic and charge transport properties and nucleation process to the absorber layer films were improved by using PMMA and maximum PCE of the device was reached to 21.6 %. In 2017, multiple cations having FA and mixed halide anions were used as absorber layers for development of the PSCs where, it was observed that the deep-level defect state concentrations were reduced due to the incorporation of iodide solution in the organic cation solution. By doing so, PCE of 19.7 % was achieved for a device having an area of 1 cm^2 and 22.1 % PCE achieved for small scale (Yang et al., 2017). In 2018, the use of Ethylene diamine tetraacetic acid (EDTA) complexed $\text{SnO}_2/\text{E-SnO}_2$ as ETL in the planar perovskite solar cells is demonstrated (Yang et al., 2018). It was observed that EDTA enhanced the device performance and PCE of 21.6 % was attained for planar PSC devices. Later in 2019, phenethylammonium iodide (PEAI) layer is used for the post-treatment of mixed perovskite ($\text{FA}_{1-x}\text{MA}_x\text{PbI}_3$) based solar cells (Jiang et al., 2019). The PEAI layer made passivate the surface defects and thereby provided higher PCE of 23.32 % for these PEAI treated PSCs. In 2020, the PCE of single junction PSCs reached 25.2 % (Green et al., 2020), which increased to 25.5 % in 2021 (Green et al., 2021). Till date, the reported PCE for the single junction perovskite solar cells is 25.7 % (NREL Best Research-Cell Efficiency Chart, 2022). In view of the efficiency enhancement, the multi-junction PSCs are needed to be investigated which are described in the next sub-section.

2.2. Multi-junction/ tandem perovskite solar cells

The Shockley Queisser limit based upon the principle of detailed balance limits PCE of the single junction devices which could be surpassed by tandem architecture. If look at the history of the tandems, initially the operating principle of multi junction/tandem devices was introduced and the concept was effectively implemented for the III-V compound semiconductors as these offer wide range of optical energy

Table 1

Brief development history of perovskite material and single junction PSCs concerned.

Year	Development detail	PCE (%)	Ref.
1839	• A mineral CaTiO_3 was discovered in Ural Mountains of Russia, Alexander Kämmerer transferred and handed-over to Gustav Rose. As per suggestion of Kämmerer, Rose named it in the name of mineralogist and politician, Count Lev Aleksevich Perovski.	-	(Katz, 2020; Rose, 1839)
1990	• Optoelectronic properties of organic and inorganic perovskites were reported.	-	(Mitzi et al., 2001)
2009	• Perovskite materials (MAPbI_3 (I) and MAPbBr_3 (II)) were used in DSSCs as liquid sensitizers where the devices are named as perovskite solar cells.	3.8 (I) 3.1(II)	(Kojima et al., 2009)
2011	• MAPbI_3 quantum dots (nanocrystalline material) were used in the perovskite solar cells.	6.54	(Im et al., 2011)
2012	• Liquid electrolyte was replaced first time by SpiroOMeTAD (HTL) in the perovskite solar cells.	9.7	(Kim et al., 2012)
2013	• MAPbI_3 PSCs were fabricated in the planar structure using two-step deposition technique.	15	(Burschka et al., 2013)
2014	• MAPbI_3 perovskite based solar cells were fabricated using two-step deposition technique. The size of MAPbI_3 cuboid was controlled which raised PCE.	17.01	(Im et al., 2014)
2015	• Li-doped mesoporous titania layer (m-TiO_2) was used as ETL in perovskite solar cells. The electronic properties and charge transportation was improved.	19.3	(Giordano et al., 2016)
2015	• MAPbI_3 was replaced by FAPbI_3 in the perovskite solar cells which improved physical properties and raised PCE.	20.1	(Yang et al., 2015)
2016	• $\text{FA}_{0.81}\text{MA}_{0.15}\text{PbI}_{2.51}\text{Br}_{0.45}$ perovskite devices were developed using VASP method.	20.5	(Li et al., 2016)
2016	• PMMA polymer was used in the perovskite solar cells.	21.6	(Bi et al., 2016)
2017	• Multiple cations and mixed halide anions were applied in the perovskite solar cells.	22.1	(Yang et al., 2017)
2018	• EDTA complexed $\text{SnO}_2/\text{E-SnO}_2$ was employed as electron transport layer.	21.6	(Yang et al., 2018)
2019	• PEAI was applied for surface defects inversion which augmented the PCE.	23.32	(Jiang et al., 2019)
2020	• The power conversion efficiency for the single junction improved, data taken from the solar cell PCE table.	25.2	(Green et al., 2020)
2021	• The PCE for the single junction was attained as revealed by PCE table.	25.5	(Green et al., 2021)
2022	• PCE to PSCs is increased as per latest NREL, USA best research cell efficiency chart.	25.7	(NREL Best Research-Cell Efficiency Chart, 2022)

band gap and lattice parameters for a variety of device applications (Yamaguchi et al., 2021; Jackson, 1958). Also for the tandems (Gee, 1988; Ludowise, 1986), the *ab initio* optical energy band-gap was calculated on the basis of detailed-balance limit (Henry, 1980). Experimentally, the fabrication of two junction (2 J) $\text{Ga}_{0.5}\text{In}_{0.5}\text{P}/\text{GaAs}$ based tandem solar cells was reported employing the metal organic chemical vapor deposition (MOCVD) method and PCE of 27.3 % was attained (Olson et al., 1990). Later, employing the same technique, PCE for the two junction (2J) InGaP/GaAs based tandems reached 30.28 % (Takamoto et al., 1997). Also for the three junction (3J) $\text{GaInP}/\text{GaInAs}/\text{Ge}$ based tandem solar cells, the theoretical PCE of 38.8 % was achieved (King et al., 2006) which raised to 40 % for the same 3J $\text{GaInP}/\text{GaInAs}/\text{Ge}$ based tandem device using a theoretical approach (King et al., 2007).

Recently, methyl-substituted carbazole monolayer has been applied as the hole-selective layer in the perovskite/Si tandem solar cells which accelerated the hole extraction and reduced the non-radiative recombination and thereby providing PCE > 29 % (Al-Ashouri et al., 2020). In due course of time, Si-based tandem devices with architectures, perovskite/Si, III-V/Si, CZTS/Si, chalcopyrite/Si and II-VI/Si could be the champion tandems with cost effectiveness (Yamaguchi et al., 2021), if one follows this work.

The tandems could be classified in three categories on the basis of electrical connections in order to extract current from both the sub-cells namely, two-terminal (2T), three-terminal (3T) and four-terminal (4T) tandem devices (Khan et al., 2022). The basic device architecture and PV operation for the tandems is explained in detail herein along with a pictorial representation in Fig. 4. In tandems, a narrower band gap sub-cell is stacked by a wider band gap sub-cell to harvest more sunlight and as a consequence, augmented performance vis-à-vis to the single junction device. In a two-terminal (2T) tandem architecture, both the sub-cells are electrically coupled via tunnel junction or recombination layer. The 2T tandem architecture needs a single transparent electrode which is advantageous since it reduces the fabrication cost by lowering the number of deposition steps and material usage. The lesser number of steps result into lower parasitic absorption in the non-active layers leading to higher potential of 2T tandems which is useful since high voltage leads to lesser resistive losses in the photovoltaic device concerned. Also during designing a 2T tandem device, certain measures need to be followed viz. (a) both the sub-cells must be fabricated in a manner that they produce parallel photocurrent since the sub-cell with lesser current would limit the overall device current and accordingly, the current matching requirement would limit the optimal energy band gap of the top sub-cell which makes the device sensitive to spectral variations, (b) the top sub-cell must be fabricated in a manner that the performance of bottom sub-cell remains unaffected, and (c) the bottom sub-cell must act as suitable substrate (Werner et al., 2018; Dupré et al., 2018).

The most simplest tandem architecture is the four-terminal (4T) tandem device architecture where, both the bottom and top sub-cells are stacked one above the other and are fabricated individually. This independent fabrication provides ease of processing and generates optimal fabrication conditions corresponding to each sub-cell, for instance, processing temperatures, top and bottom sub-cell polarities, substrate roughness and proper use of solvents. The 4T tandem devices are operated via four electrical connections, out of these, at least three should show high transparency in wide spectral range and one of these in the infrared range. In a 4T device, both the sub-cells are kept under operation independently which makes the device less sensitive to spectral variations and reduces choice limitation to top sub-cell band gap. Consequently, 4T device attains high PCE corresponding to a wide range of top sub-cell band gaps which makes the device architecture free from current matching as well (Werner et al., 2018; Dupré et al., 2018).

One important aspect of the 2T tandems is the phenomenon of luminescent or radiative coupling, basically re-absorption of luminescent photons by the bottom sub-cell which are emitted from the top sub-cell. Jäger et al. (Jäger et al., 2021) reported theoretically an impact of bifacial illumination and luminescent coupling on the performance of 2T perovskite/silicon tandems by employing an idealized solar cell model for the top perovskite sub-cell, Shockley-Queisser limit based upon detailed balance and Richter limit for the bottom Silicon sub-cell. Accordingly, predicted that an additional backside illumination of about 10–20 % which was enough to alter the optimum top sub-cell band gap from 1.71 eV to 1.6–1.64 eV range. The luminescent coupling could significantly decrease current mis-matching as revealed. The luminescent coupling in 2T perovskite/Silicon tandems boosted flexibility in sub-cell thickness and increased tolerance against various spectral conditions along with reduced current mis-matching (Bowman et al., 2021).

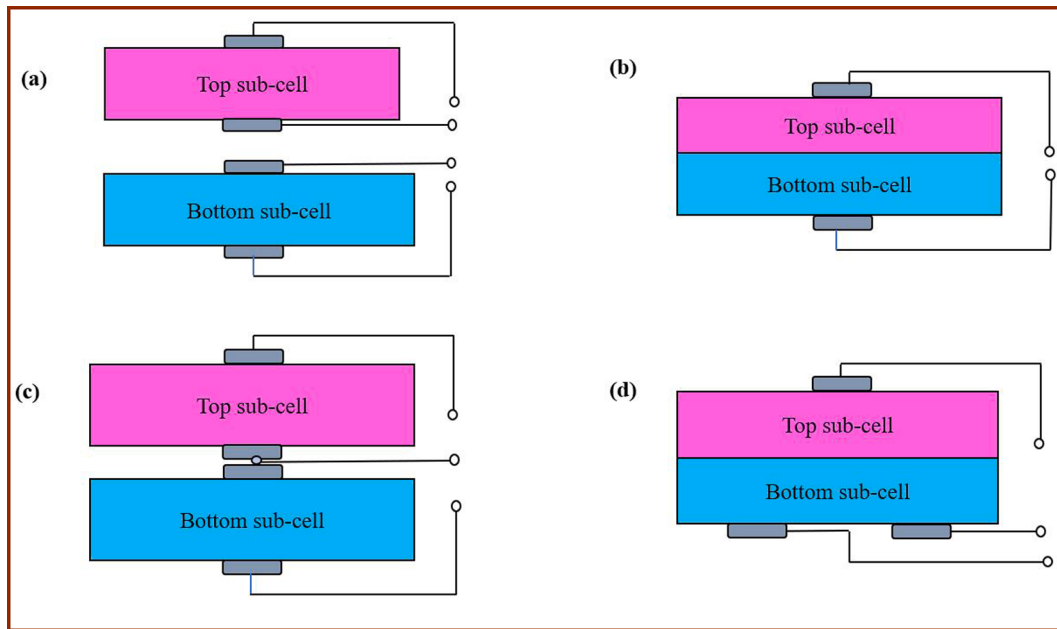


Fig. 4. Typical illustration of electrical connections for (a) four-terminal (4T), (b) two-terminal (2T), (c) three-terminal (3T) middle and (d) three-terminal (3T) IBC tandem devices.

As stated, the 2T tandems suffer from the drawback of current mismatching whereas 4T devices face issues such as higher fabrication costs and optical losses. These can be overcome by employing 3T tandems where three terminals are required for current extraction (Khan et al., 2022). In this architecture, top and bottom sub-cells are typically comprised of front and back contacts while for current extraction from the third terminal is made either through an interdigitated back contact (IBC) added in bottom sub-cell or by middle contact added between top and bottom sub-cells. Under PV operation, the maximum power can be extracted from the 3T device with no current mis-matching (Schnabel et al., 2020; Warren et al., 2020). Reports are available so far on the perovskite-based tandems comprising of perovskite based top sub-cell while in all perovskite tandems, both the sub-cells are perovskite based. In 2014, perovskite/kesterite ($\text{Cu}_2\text{ZnSn}(\text{S},\text{Se})_4$) monolithic tandem device with architecture Glass/Mo/ $\text{Cu}_2\text{ZnSn}(\text{S},\text{Se})_4/\text{CdS}/\text{ITO}/\text{PEDOT:PSS}/\text{CH}_3\text{NH}_3\text{PbI}_3/\text{PCBM}/\text{Al}$ is reported (Todorov et al., 2014) with PCE 4.6 % whereas for the same tandem architecture, PCE of 16 % was predicted employing simulation modeling by the same group. In 2015, the semi-transparent Ag nanowire electrodes were demonstrated (Bailie et al., 2015) where PSC based top sub cell was mechanically stacked onto bottom CIGS and Silicon sub-cells by achieving PCE 17 % and 18.6 %, respectively for Perovskite/Si and Perovskite/CIGS architectures.

Later in 2016, Eperon and coworkers (Eperon et al., 2016) studied monolithic two terminal (2T) and mechanically stacked four terminal (4T) tandems combining low band gap $\text{FA}_{0.75}\text{Cs}_{0.25}\text{Sn}_{0.5}\text{Pb}_{0.5}\text{I}_3$ and high band gap $\text{FA}_{0.83}\text{Cs}_{0.17}\text{Pb}(\text{I}_{0.5}\text{Br}_{0.5})_3$ perovskites. They attained better PCE 20.3 % for 4T tandem device and lower 17 % for 2T devices. 2T architected monolithic perovskite/Si tandems demonstrated higher PCE of 23.6 % in 2017 by combining bottom Silicon based sub-cell with top Cesium formamidinium lead halide based perovskite sub cell (Bush et al., 2017) which showed better stability. The PCE is further augmented for perovskite/Si tandems in the year 2018 by attaining 28 % which overcome highest PCE of the single junction Silicon solar cell device (Oxford PV perovskite solar cell achieves 28% efficiency, 2018). Typical device architecture to a perovskite/Si tandem is embraced in Fig. 5 where perovskite sub-cell is implicated as top sub-cell and Si based sub-cell as bottom. The modified tandem architecture could undertake a

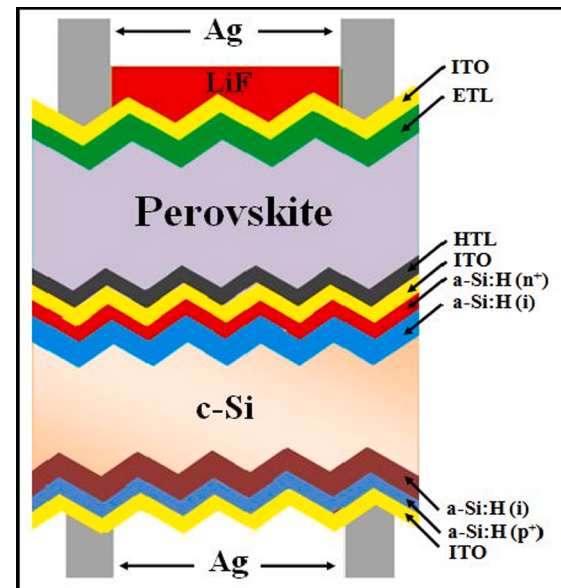


Fig. 5. Graphical representation of a typical two terminal two junction bifacial perovskite/Si tandem solar cell device.

breakthrough not only in surpassing the PCE but in stability too where persistent efforts are made so far by varying device design and materials evolution.

Recently (NREL Best Research-Cell Efficiency Chart, 2022), the recorded PCE has approached to 31.3 % and 24.2 %, respectively for perovskite/Si and perovskite/CIGS monolithic tandems. The graphical representations as year wise bar diagrams to the attained PCEs for single junction PSCs and tandems concerned are depicted in Fig. 6 (a-c) along with their comparison. The next section deals with the structure of the perovskite materials and the factors determining the stability and PCE of the PSCs.

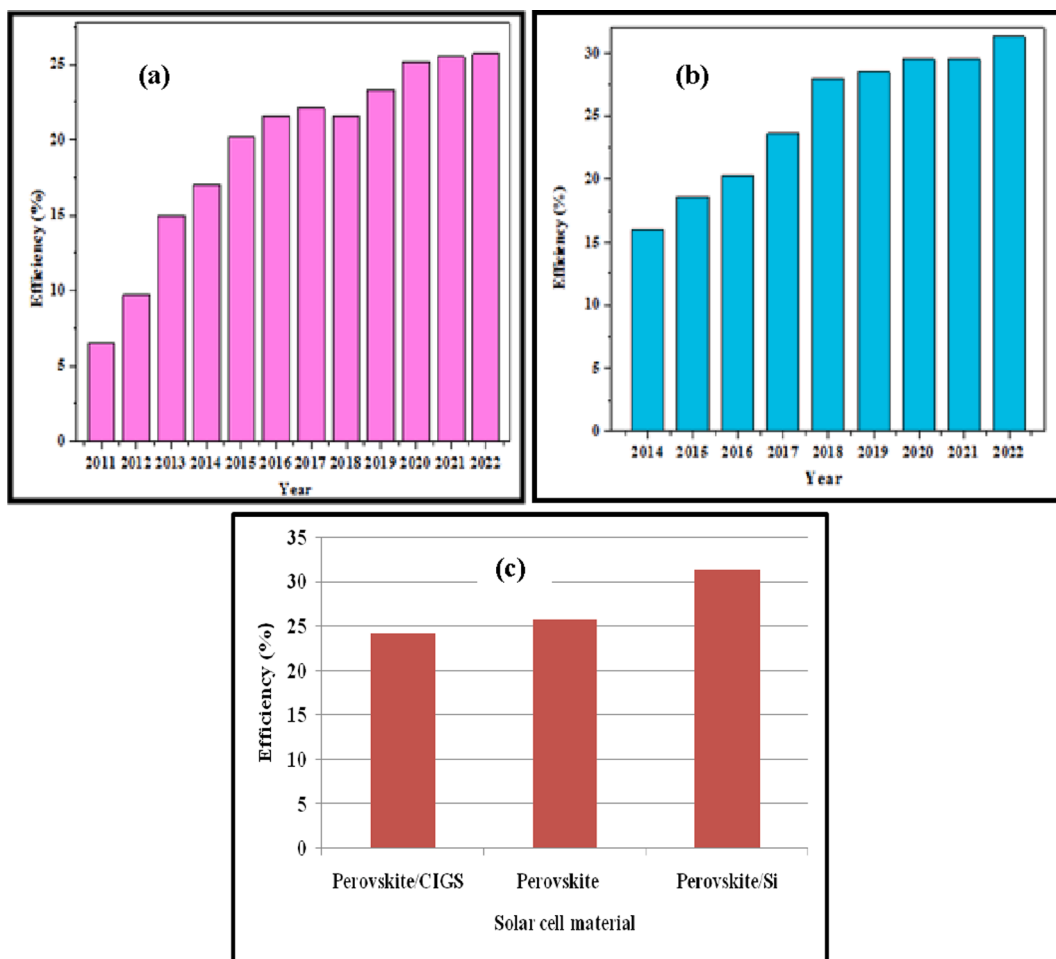


Fig. 6. 2-D bar diagram representing (a) PCE for the single junction PSCs during 2011–2022, (b) PCE for PSC based tandems during 2014–2022 and (c) an overview for the single junction PSC's PCE along with tandems concerned.

3. Structure of perovskite materials

As discussed earlier, the group of compounds having general crystal formula ABX_3 are known as perovskites where both the A and B are cations and X is an anion usually taken halogen(s) for the target domain herein. The unit cell of a basic ABX_3 perovskite is represented in Fig. 7. Although the perovskite materials have been applied so far in a variety of applications yet in view of solar cell devices, two types of halide perovskites are typically applied as (a) Alkali and (b) Organic-inorganic based halide perovskites. Alkali based halide perovskites have alkali monovalent cation (A), divalent cation (B) and halogen anion (X). Herein, Cesium (Cs^+), Rubidium (Rb^+), Potassium (K^+), Sodium (Na^+) and Lithium (Li^+) are taken as (A), Lead (Pb^{2+}), Tin (Sn^{2+}) and Germanium (Ge^{2+}) as (B) and Chlorine (Cl^-), Bromine (Br^-), Iodine (I^-) and Fluorine (F^-) as halogens (X). Organic-inorganic based halide perovskites comprise organic monovalent cation (A) where Methylammonium ($CH_3NH_3^+$), Ethyl ammonium ($CH_3CH_2NH_3^+$) and Formamidinium ($NH_2CHNH_2^+$) are taken as monovalent cation (A) (Kim et al., 2014a; Luo et al., 2021; Asghar et al., 2017).

The structure and phase of perovskite materials are strongly affected by environmental conditions like temperature, moisture, pressure etc. which in turn affect stability of the PSCs (Niu et al., 2015). In solar cell devices, most commonly used perovskite so far is Methylammonium lead iodide ($CH_3NH_3PbI_3$) which is having Methylammonium ($CH_3NH_3^+$) as cation but, it has volatile nature and could be replaced by Formamidinium (Wali et al., 2020; Noh et al., 2013a; Stoumpos et al., 2013). However due to its large size, Formamidinium is not structurally

stable and has not tendency to form black perovskite phase unlike Methylammonium, rather it undergoes a phase transformation at room temperature (Baena et al., 2017a).

Since, the perovskite materials have akin crystal structure to that of the Calcium Titanate ($CaTiO_3$) where cations and anions form cubic and octahedral geometries. An ideal perovskite must be structurally stable (Roy et al., 2020; Kim et al., 2014a; Luo et al., 2021; Asghar et al., 2017) provided it satisfies Goldschmidt tolerance and octahedral factors which are responsible for determination of the stability.

(a) Goldschmidt tolerance factor (t)

The perovskite structure is comprised of different constituent elements/ions dealt with isomorphism theory that explains similarity in crystalline structure between chemical compounds. The crystalline structure of perovskite mineral was primarily illustrated by mineralogist, Victor Goldschmidt in his work which was undertaken on tolerance factors and led to additional progress in isomorphism theory (Katz, 2020; Park et al., 2016; Goldschmidt, 1926), later recognized as Goldschmidt's rule which also suggests that absolute isomorphism could be achieved only between atoms whose ionic radii are not changed more than 10–15 %. Goldschmidt's tolerance factor as mentioned by Eq. (1) was previously formulated to explain perovskite structure (Katz, 2020; Rose, 1839; Bartel et al., 2019) and nowadays, it is used for determining the stability of ionic crystal structure too.

$$t = \frac{R_A + R_X}{\sqrt{2(R_B + R_X)}} \quad (1)$$

Here, R_A , R_B and R_X are the ionic radii to the cations A and B and

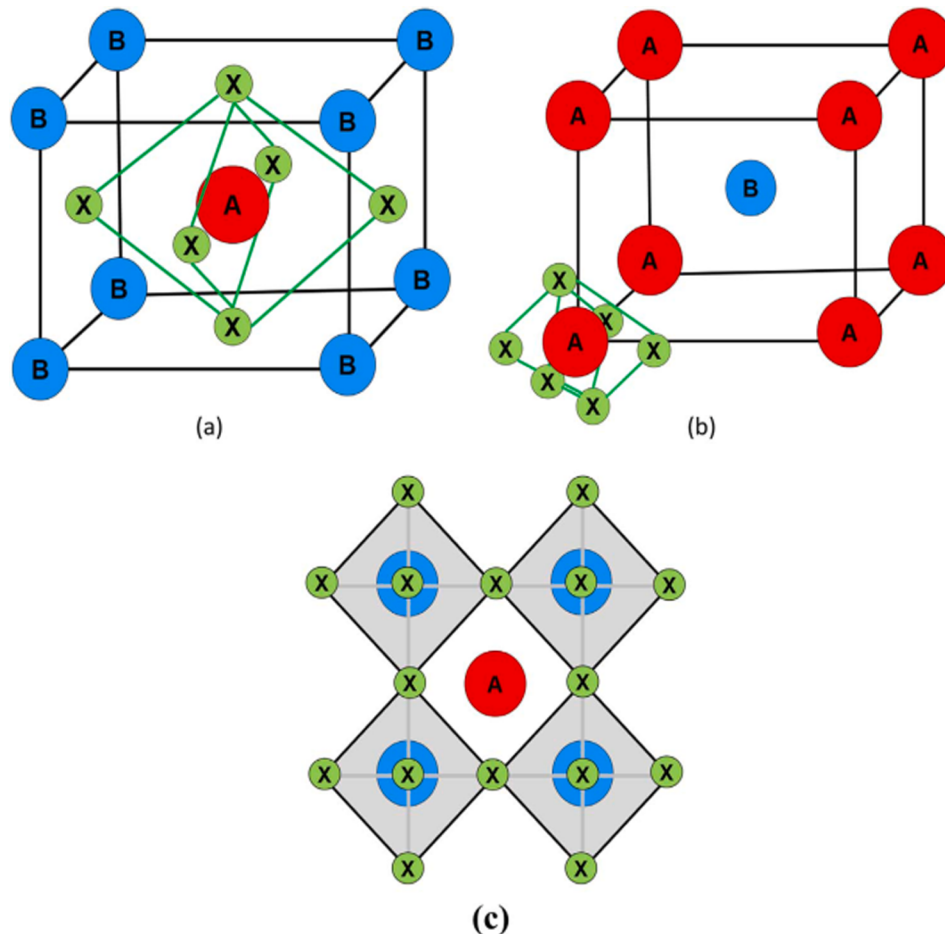


Fig. 7. 3D structure of unit cell to ABX_3 cubic perovskite wherein structures have (a) B at $<0,0,0>$ position, (b) A at $<0,0,0>$ position and (c) BX_6 octahedral structure. Reprinted with permission from Ref. (Asghar et al., 2017) Copyright (2017) Elsevier Ltd.

anion X, respectively. Usually for all the perovskites, tolerance factor typically lies within 0.75–1.00 (Li et al., 2008). It lies within 0.9–1.0 for the cubic perovskite structure and lesser or greater range vis-à-vis to cubic confirms hexagonal, orthorhombic, tetragonal, rhombohedral structures (Fu et al., 2018; Poglitsch and Weber, 1987; Stoumpos et al., 2013). It is not a sufficient condition for demonstrating complete stability in perovskites and thus, consideration of octahedral factor is also necessary (Li et al., 2004) which is addressed in the following section.

(b) Octahedral factor (μ)

Octahedral factor which is represented in Eq. (2), determines distortion and stability in the perovskites. For a stable structure, it must lie within 0.45–0.89 range (Roy et al., 2020; Travis et al., 2016; Mitzi et al., 1999) where symbols are abbreviated in the earlier sub-section.

$$\mu = \frac{R_B}{R_X} \quad (2)$$

The next section presents properties of the perovskite materials along with their chemical stability under different environmental conditions.

4. Properties and chemical nature

4.1. Properties

The halide based perovskite materials are considered as desirable materials for the solar cell applications due to their attractive properties such as high absorption coefficient, optimum and tunable band gap, suitable electron and hole transportation, higher diffusion carrier length and electron mobility, lower surface recombination velocity and exciton

binding energy, higher carrier lifetime and photoluminescence along with greater structural defect tolerance. These properties can be tailored by controlling concentration to constituent cations and anions along with shape and size of the perovskite materials which make these useful for development of the perovskite based solar cells (Roy et al., 2020; Nair et al., 2020; Yang et al., 2019; Valverde-Chavez et al., 2015; Xing et al., 2014; Gonzalez-Pedro et al., 2014; Djurisic et al., 2017; Hirasawa et al., 1994; Minemoto and Murata, 2014).

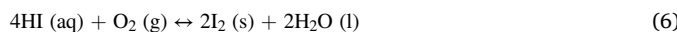
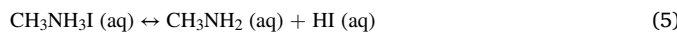
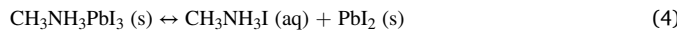
4.2. Chemical nature

The chemical stability of a perovskite structure under different environmental conditions plays vital role in determining the durability and sustainability to the perovskite-based devices (Niu et al., 2015; Poorkazem and Kelly, 2017; Kundu and Kelly, 2018; Niu et al., 2014; Letcher and Fthenakis, 2018). The organo-metallic perovskites have undergone through a chain of chemical reactions under varied environmental conditions and degraded directly either into components concerned or other chemicals. The chemical reaction dealing with Methylammonium lead iodide ($\text{CH}_3\text{NH}_3\text{PbI}_3$) perovskite is as:



Herein, the double-sided arrow indicates reversible reaction that is, sometimes product obtained may be degraded into components concerned leading to backward reaction and as a consequence, the perovskite material is decomposed (Wang et al., 2016a; Niu et al., 2015; Gujar et al., 2018). In presence of water and Oxygen, the degradation mechanism is given by Eqs. (4)–(7) (Wang et al., 2016a; Niu et al., 2015; Gujar

et al., 2018; Han et al., 2015; Domanski et al., 2018).



At second stage to the reaction represented by Eq. (5), $\text{CH}_3\text{NH}_3\text{I}$ degrades into CH_3NH_2 and HI and in third stage by Eq. (6), HI further degrades in presence of Oxygen or may degrade into H_2 and I_2 as given by Eq. (7). The $\text{CH}_3\text{NH}_3\text{PbBr}_3$ and $\text{CH}_3\text{NH}_3\text{PbI}_2\text{Cl}$ perovskites also undergo similar degradation mechanisms but, the reactants are differed. The device architecture is so important to achieve desired PCE in solar cells along with stability and thus, the next section describes it.

5. Device architecture to single junction perovskite solar cells

The solar cell device is typically a p-n junction which comprises substrate, front and rear electrodes, optical window and absorber layers. The optical window creates an asymmetric junction with the absorber and drives the generated charge carriers towards electrodes concerned. In order to enhance power conversion efficiency of a device, different architectures have been employed so far in substrate and superstrate structures. The PCE to PSCs also depends on device architecture (mesoporous and planar) and growth recipes along with pre- and post-treatments to the constituent layers. Mesoporous structure requires high annealing temperature for fabrication of constituent layers and as a result, process becomes time consuming and hence, researchers started exploring planar device architectures concerned (Xing et al., 2013). Typically, two types of device architectures are reported for PSCs so far viz. (a) planar structure (*n-i-p*) and (b) inverted structure (*p-i-n*) (Kumari et al., 2018a) as depicted in Fig. 8.

Typical planar and inverted planar architectures are Glass/TCO/ETL/Perovskite/HTL/Metal contact and Glass/TCO/HTL/Perovskite/ETL/Metal contact, respectively (Song et al., 2016; Jeng et al., 2014; Eperon et al., 2014a; Liu et al., 2013; Jeng et al., 2013). In a planar superstrate structure (*n-i-p*), ETL is coated first onto transparent conducting oxide (TCO) coated glass substrate like Fluorine doped Tin oxide

(FTO) and Indium doped Tin oxide (ITO) coated glass substrates followed by coating the perovskite absorber layer and then HTL. The device development is ended by depositing suitable metal contacts which work as rear electrode. A variety of materials are optimized so far for the constituent layers and electrodes which are having their own merits and demerits. For the ETL, commonly used materials are Titanium Oxide (TiO_2), Tin Oxide (SnO_2), Zinc Oxide (ZnO), [6,6]-Phenyl-C₆₁-Butyric acid Methyl Ester (PCBM) etc. while 2,2',7,7'-tetrakis[N,N-di(4-methoxyphenyl)amino]-9,spirobifluorene (SpiroOMeTAD), Poly (3-hexylthiophene) (P3HT), NiO_x are employed so far as HTL. The electrode materials like Aluminum (Al), Silver (Ag), Gold (Au), Molybdenum (Mo) or Carbon (C) are typically applied based upon their advantages in order to achieve better performance to the devices (Noh et al., 2013b; Luo et al., 2015; Xu et al., 2016a; Sheng et al., 2015; Wu et al., 2015; Chen et al., 2014).

In an inverted structure, HTL is coated onto TCO substrate followed by perovskite absorber and ETL and ended with electrode/metal contact deposition. In this architecture, commonly used materials for ETL and HTL are PCBM and Poly(3,4-ethylenedioxythiophene) Polystyrene Sulfonate (PEDOT:PSS), respectively (Park et al., 2016; Kim et al., 2014b; Heo et al., 2015; Ciro et al., 2017; Chiang et al., 2014), while other materials may also be applied as discussed above. Pre- and post-treatments to the constituent layers are also undertaken in order to develop better devices while, proper selection of constituent layers is so important to achieve pretty performance with desired stability and persistent efforts are made so far across the globe ever since its invention in 2009. In superstrate architecture, solar irradiance enters from the glass side while in substrate structure, the base is an opaque and irradiance illuminates directly over the device where both the structures are having their own advantages along with differently configured development and characterization tools. In superstrate architecture, bottom layer must be transparent while the top layer must have good contact with electrodes, otherwise dark current may be increased and resulted into reducing the device performance. Also, the top layer must properly cover the perovskite layer, reduce the defects and must be treated at low temperatures, as high temperature could decompose perovskite absorber. Since, all the layers play an important role in the devices and therefore, the following sub-section describes the ETLs in detail comprising of organic and inorganic classifications.

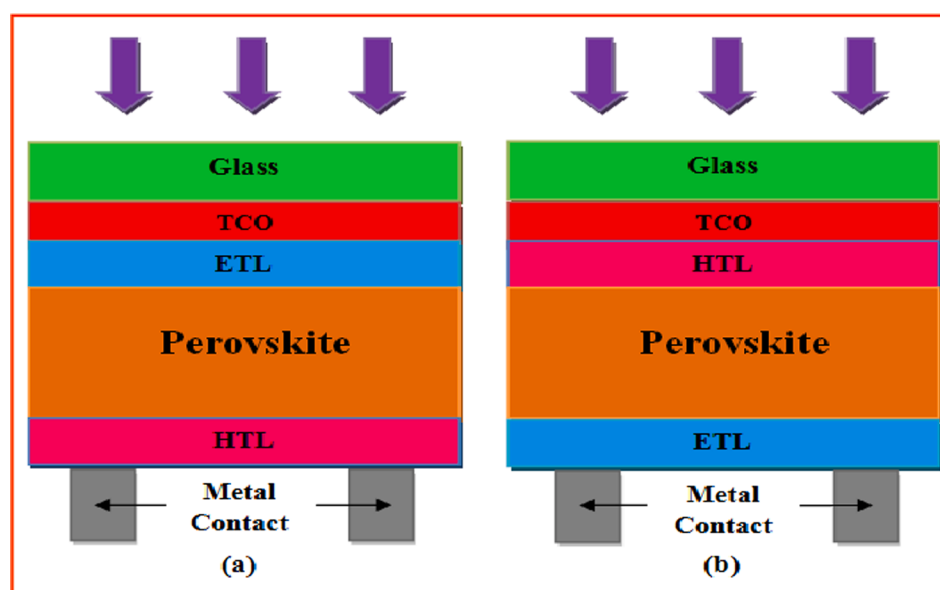


Fig. 8. Typical device architectures for the PSCs in (a) *n-i-p* and (b) *p-i-n* configurations.

5.1. Electron transport layer (ETL)

The electron transport layer (ETL) transports generated electrons in perovskite absorber layer and sometimes it also blocks holes and hence, selection of an appropriate ETL is important (Letcher and Fthenakis, 2018). Initially, mesoporous or planar TiO_2 are widely used as ETL in the PSCs due to its lower cost, easy processing, suitable energy band gap and large electron lifetime along with faster charge transfer rates (Kojima et al., 2009; Gubbala et al., 2008). Later, organic and inorganic or metal oxide ETLs like PCBM, TiO_2 , ZnO , Al_2O_3 , ZrO_2 , SnO_2 , SiO_2 etc. are existed. Although organic ETLs have decent charge carrier mobility, suitable energy level alignment and low temperature requirements (Chiang et al., 2014; Docampo et al., 2013a) yet inorganic ETLs are preferred over organic ones due to their higher stability and lesser cost. The study of varied ETLs is crucial for the perovskite solar cell devices concerned and accordingly, the next sub-section provides a description about inorganic ETLs.

5.1.1. Inorganic ETLs

The first ever reported PSC was comprised of an inorganic ETL where Kojima and others (Kojima et al., 2009) used TiO_2 as an ETL and attained PCE 3.81 % and 3.1 %, respectively for the MAPbI_3 and MAPbBr_3 which was followed by others with materials evolution (Poglitsch and Weber, 1987; Lin et al., 2021; Docampo et al., 2013b; Im et al., 2011) by reporting improved PCE. Subsequently, photovoltaic performance of PSCs was analyzed with and without *meso*- TiO_2 where devices without *meso*- TiO_2 ETL demonstrated more stability whereas devices with *meso*- TiO_2 were found instable under UV illumination (Rombach et al., 2021). In 2015, Kim et al. (Kim et al., 2015a) used compact $\text{TiO}_2/\text{c-TiO}_2$ in the PSC devices and achieved higher PCE of 12.2 %. Later, in 2018, an enhanced PCE of 16.75 % was attained using TiO_2 as ETL (Chen et al., 2018). Nonetheless, TiO_2 is undoubtedly the most commonly used electron transport material (ETM) but, under UV illumination, oxygen vacancies are generated due to reaction of photo-induced holes and oxygen radicals consequently, ETL is degraded and thus, alternative ETMs are required (Kim et al., 2016; Leijtens et al., 2013). ZnO became widely used ETM with higher stability and electron mobility, lower temperature requirements and more favourable alignment with the commonly used MAPbI_3 perovskite in PSC devices (Meulenkamp, 1999; Mahmood et al., 2014; Tseng et al., 2015; Siempelkamp et al., 2015). Nowadays, ZnO nanoparticles (NPs) and nanorods are also in use as ETM which have showed an alternate replacement to *meso*- TiO_2 as ZnO NPs based layers could be processed at low temperatures too (Dong et al., 2014; Liu and Kelly, 2014; Son et al., 2014). The ZnO NPs have been applied as ETL by achieving PCE of 18.9 % with better stability vis-a-vis to TiO_2 ETL based devices (Song et al., 2017). The TiO_2 and ZnO ETLs have also been followed by doping where *n*-type doping showed better performance as compared to the *p*-type which led to decreased charge recombination and increased electron transport resulted into better performance. In 2014, the use of Al-doped ZnO (Al:ZnO) nanorods demonstrated (Dong et al., 2014) desired PCE by getting 8.5 % without and 10.7 % with doping. The drawbacks of chemical instability in ZnO at low temperatures and as stated earlier for TiO_2 like lower electron mobility, higher temperature requirement and instability in the UV region (Docampo et al., 2013a; Meulenkamp, 1999; Baena et al., 2017b) invited potential for replacement and later on, SnO_2 has been demonstrated as efficient ETL owing to its higher transparency, stability in UV region and electron mobility along with better band gap alignment with perovskite absorber (Wang et al., 2016b; Dong et al., 2017). The SnO_2 ETL was used in the $\text{CH}_3\text{NH}_3\text{PbI}_3$ based PSCs and PCE of 17.21 % was achieved (Ke et al., 2015). Li and others (Li et al., 2015) used SnO_2 NPs as ETL in the $\text{CH}_3\text{NH}_3\text{PbI}_3$ based perovskite solar cells and attained PCE of 10.18 %. Along with the inorganic ETLs, organic materials have also been employed so far as efficient ETLs which are deliberated in the following section.

5.1.2. Organic ETLs

Organic ETLs like fullerene (C_{60}) and its derivatives like PC_{70}BM , Indene- C_{60} Bissaduct(ICBA), ThCBM, PC_{71}BM , and PC_{61}BM are widely used in inverted (p-i-n) structures due to their tunable band gap and high electron mobility (Jeng et al., 2014; Kim et al., 2014b; Heo et al., 2015; Ciro et al., 2017; Chiang et al., 2014; Gubbala et al., 2008). The fullerene derivatives PC_{61}BM and PC_{71}BM have been employed as ETLs in the $\text{CH}_3\text{NH}_3\text{PbI}_3$ based PSCs, where 9.92 % and 16.32 % PCEs were attained for PC_{61}BM and PC_{71}BM , respectively (Chiang et al., 2014). The planar $\text{CH}_3\text{NH}_3\text{PbI}_3$ based PSCs were reported where perovskite absorber layer was fabricated using solution processed method and fullerene as ETL by attaining PCE of 12.21 % (Xu et al., 2016b). A new organic ETL TDTP was introduced by Gu and group (Gu et al., 2017) as an alternative to PCBM ETL and achieved higher PCE of 18.2 % (). Wang and coworkers (Wang et al., 2014) spin coated fullerene bilayer on the perovskite layer by using mixed solution of PCBM and ICBA and obtained PCE of 12.2 %. Later in order to achieve better stability, combination of bilayers (2 ETLs) like $\text{SnO}_2/\text{TiO}_2$, SnO_2/ZnO , TiO_2/ZnO etc was applied. The use of TiO_2/ZnO bilayers in the MaPbI_3 based PSCs (Kumari et al., 2018b) is reported by attaining PCE of 6.51 %. An impact of TiO_2/ZnO bilayer ETL on PSCs was undertaken by spin coated TiO_2 sol-gel and then ZnO sol-gel. The complete device presented enhanced PCE of 17.2 %, while single ZnO ETL showed PCE 13.2 % only (Xu et al., 2015). The $\text{SnO}_2/\text{TiO}_2$ bilayers developed by NPs suspension at low temperature and applied as ETL, attained greater PCE of 15.2 % whereas the single TiO_2 ETL presented PCE of 14.9 % (Denegri et al., 2018). In inorganic ETLs, SnO_2 gained maximum attention due to its improved stability and PCE whereas among organic ETLs, PCBM is widely used but, its stability is a concern since it gets degrade easily. Similar to the ETLs, the HTLs also play significant role in the perovskite device development along with interface engineering and therefore, the following sub-section describes importance of various HTLs applied so far in perovskite devices by classifying these as inorganic, organic and polymeric HTLs.

5.2. Hole transport layer (HTL)

Hole transport layer plays a vital role in determining the stability and PCE of perovskite solar cells since, both the stability and PCE also depend significantly on the applied HTL to the device. During the selection of an appropriate hole transport material (HTM), certain parameters need to be taken into consideration such as high thermal stability and hole mobility, good light to power conversion efficiency, cost effectiveness, ease of fabrication and lesser sensitivity towards humidity and air (Yu and Sun, 2015; Bakr et al., 2017). As stated, the hole transport layers are classified in three types namely: inorganic, organic and polymeric HTLs (Rombach et al., 2021; Wang et al., 2017; Sun et al., 2016; Christians et al., 2014). The detailed relevant works reported so far are depicted in the following sub-sections along with their roles and merits.

5.2.1. Inorganic HTLs

Initially CZTS was widely applied worldwide as an inorganic HTL which gained tremendous attention. Wu and others (Wu et al., 2015) used recyclable and inorganic CZTS NPs in PSC device structure and obtained PCE of 12.75 %. The CZTS NPs were synthesized under ambient conditions, spin coated as thin film layers and applied as HTLs in perovskite devices by achieving PCE 9.66 % (Patel et al., 2018) and 15.4 % (Khanzada et al., 2016). Nickel oxide (NiO_x) is another popular inorganic HTM found in abundance having desirable properties like better chemical stability, lower cost and desired optical energy band gap. It is used as HTL in PSCs which attained PCE of >20 % (Kim et al., 2015b; Xie et al., 2017). Tang et al. (Tang et al., 2018) used NiO nanocrystals (NCs) of varying thickness viz. 30 nm, 55 nm, 70 nm, 100 nm and 170 nm as HTM in inverted planar device architecture to the PSCs. In order to present topography and morphology, TEM and SEM images are depicted in Fig. 9 for pristine and annealed NiO samples. The

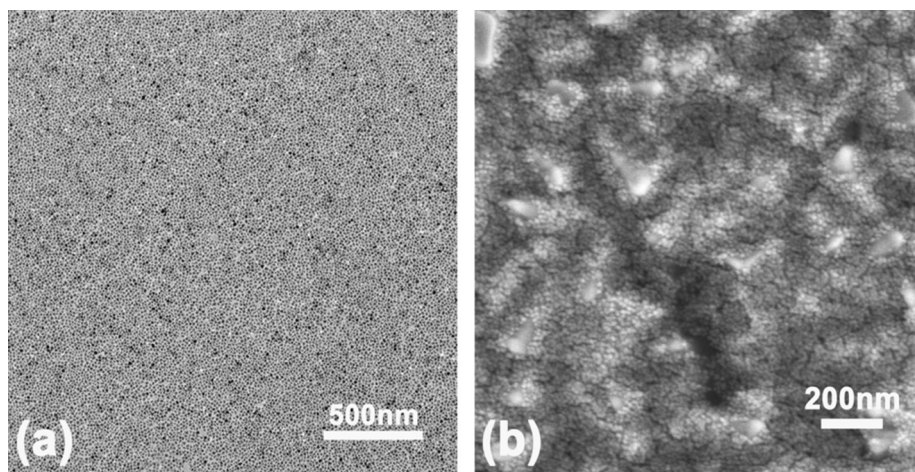


Fig. 9. (a) TEM image of pristine NiO and (b) SEM image of 500 °C annealed NiO samples. Reproduced with permission from Ref. (Tang et al., 2018) Copyright (2017) Elsevier Ltd.

pristine NiO TEM image showed well dispersed NCs and annealed NiO SEM image showed uniform dispersion of NCs. The NiO NCs with thickness 55 nm attained better PCE of 15.47 % vis-à-vis to the others.

5.2.2. Organic HTLs

Among the organic HTLs, SpiroOMeTAD has been extensively used so far due to its suitable ionization potential and wide absorption spectrum (Nair et al., 2020; Rombach et al., 2021). To enhance PCE and stability to PSC device, SpiroOMeTAD was applied as organic HTL and replaced the liquid electrolyte. In order to increase charge carriers, SpiroOMeTAD is usually doped with Li-TFSI (Lithium salt) but, hygroscopic nature of this dopant reduced stability of the device (Kim et al., 2012). The fabrication of spirobifluorene core in spiroOMeTAD molecules not only requires large scale synthesis process which makes it costly but symmetric structured spiroOMeTAD molecules crystallize at high temperatures, affect charge transport properties and long term stability of the devices too (Malinauskas et al., 2015). In 2018, the SpiroOMeTAD implication as HTL resulted into higher PCE of 22 % but, still stability and cost are the drawbacks those need to be overcome (Wang et al., 2016a; Maniarasu et al., 2018). Later, SpiroOMeTAD was replaced by novel HTM, Nickel phthalocyanine (NiPc) by undertaking work on both the stability and PCE aspects where PCE was attained 12.2

% with boosted stability where the normalized efficiency decay curves to both the primary and novel HTM as discussed are shown in Fig. 10 which demonstrated that PSCs with NiPc HTL retained 80 % of the initial PCE after storage of 38 days whereas SpiroOMeTAD HTL retained only half of the initial PCE after 12 days storage (Haider et al., 2018).

The cost effectiveness, stability and power conversion efficiency to the PSCs invited attention of the workers potentially for efficient alternatives and accordingly, polymeric materials are demonstrated as hole transport materials which are discussed in the following sub-section.

5.2.3. Polymeric HTLs

Among the polymeric HTLs, the P3HT (thiophene based molecule) and Poly(triaryl amine) (PTAA) are the most commonly used materials. Although P3HT has good hole conductivity with cost effectiveness yet it has lower PCE vis-à-vis to the PTAA. Since carrier density and mobility are important parameters and to enhance these, P3HT has been incorporated with Li-TFSI and tBP so far (Chen et al., 2018; Nia et al., 2017; Chen and Yang, 2016). To improve the charge carrier transport, persistent efforts have been made by removing the HTL in PSCs and by introducing a buffer layer and organic monolayer based PSC device demonstrated PCE of 19.4 % (Wang et al., 2019). In 2018, molecular doped F4TCNQ was performed with perovskite absorber layer in HTL free PSCs by achieving PCE of 20.2 % where device fabrication process not only became simple but cost effective too (Wu et al., 2018).

Nonetheless, inorganic HTLs have fair opto-electronic properties and stability but, none of these materials have outdated organic HTLs while on the other hand, organic HTLs have good stability but not cost effective. Polymeric HTLs provide only marginal enhancement in the performance of the devices while HTL free devices face severe drop in charge transport due to mis-matched energy levels of ETL and perovskite layer. Hence nowadays, the main focus is to implicate an amalgamation of two different HTMs for the modification in PCE along with stability. Carbon based HTMs such as single walled carbon nano tubes (SWCNT) and graphene are used solely with organic HTM SpiroOMeTAD and attained PCE of 15.5 % (Aitola et al., 2016). An overview on types, merits and demerits to various ETLs and HTLs is provided in Table 2 for better understanding.

In a solar cell device, the absorber layer plays principal role where incident irradiance gets absorb by generating charge carriers viz. electrons and holes. An efficient absorber layer should harvest maximum incident spectra by utilizing its maximum fraction in charge carrier generation. Therefore, next section is devoted to the perovskite absorbers which are employed so far in the solar cell device development.

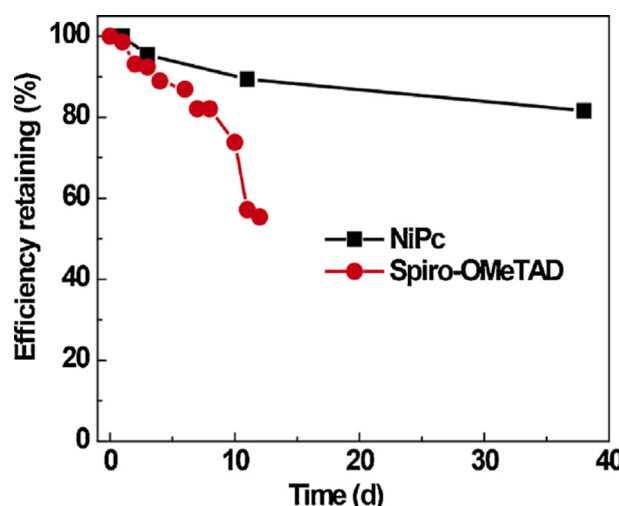


Fig. 10. Normalized efficiency decay curves for PSCs embracing NiPc and SpiroOMeTAD as HTL. Reprinted with permission from Ref. (Haider et al., 2018) Copyright (2018) Elsevier Ltd.

Table 2

Types, merits and demerits to Electron Transport Layers (ETLs) and Hole Transport Layers (HTLs) which are employed so far in perovskite solar cells.

Types	Merits	Demerits	Ref.
Organic ETLs (PCBM, ICBAs, ThCBM etc.)	• Can be used at low temperatures, and having suitable band gap and good electron mobility.	• Stability issues.	(Jeng et al., 2014; Kim et al., 2014b; Heo et al., 2015; Ciro et al., 2017)
Inorganic ETLs (TiO ₂ , ZnO, Al ₂ O ₃ , ZrO ₂ , SnO ₂ , SiO ₂ etc.)	• Simple fabrication and cost effective, having suitable band gap with longer lifetime and their bilayers are applied to attain higher PCE.	• Requires high temperatures and these are having low electron mobility.	(Kojima et al., 2009; Gubbala et al., 2008; Baena et al., 2017b)
Organic HTLs (SpiroOMeTAD)	• Suitable ionization potential and wide absorption spectrum.	• Hygroscopic nature and stability issues with higher cost.	(Nair et al., 2020)
Inorganic HTLs (CZTS, NiO _x etc.)	• Chemically stable, economically viable and eco-friendly and provides higher performance.	• PCE and stability are still lower vis-à-vis to organic HTLs.	(Chen et al., 2018; Wang et al., 2017; Sun et al., 2016; Christians et al., 2014)
Polymeric HTLs (P3HT, PTAA etc.)	• Good environmental stability.	• Higher cost and lower PCE.	(Chen et al., 2018; Nia et al., 2017; Chen and Yang, 2016)

5.3. Perovskite thin film absorber layers

In device architectures employed so far for the perovskite solar cells, the perovskite based absorber is sandwiched between the hole and electron transport layers where following transport layers development and treatment may also impact it. The perovskite thin film absorber layers must be fabricated using appropriate fabrication techniques to achieve desirable physical properties. The optoelectronic properties to perovskite thin films are correlated with the morphology, crystallinity, stoichiometry etc. which could be altered by development routes, techniques, doping, pre-and post-treatments, ambients, solvents and molar compositions (Docampo et al., 2013b; Dualeh et al., 2014; Cho and Park, 2017; Cao et al., 2019). In perovskite devices, typically physical and chemical routes are employed including vapor deposition method and one- and two-step solution based methods which are deliberated herein. The methods are classified as vapor, solution, hybrid and diffusion where in vapor process, the absorber layer is developed by evaporation method either co-evaporation or sequentially, in solution process, the absorber layer is totally fabricated by spin coating (one-step) along with dip coating (two step), in hybrid process, it is deposited by both the solution and vapor processes and in diffusion process, partially developed either by vapor or solution process and then, the samples is kept in a graphite block at elevated temperature comprising of compound to be diffused.

5.3.1. Vapor deposition method

The thermal evaporation method has been typically employed to develop perovskite absorber layers where two source holders are separately used for CH₃NH₃I and PbI₂ which are controlled by two different thermocouples and this is categorized as co-evaporation technique. It was initially employed for preparation of mixed/hybrid CH₃NH₃PbI_{3-x}Cl_x perovskite where perovskite absorber was fabricated via co-evaporation of CH₃NH₃I and PbCl₂ on meso-TiO₂ films followed by annealing and deposition of HTL and then the device was ended with

metal contact formation where the achieved PCE was 15.4 % (Liu et al., 2013). The drawback of this technique is that it requires high vacuum for the deposition process which increases the operational cost as well. For development of the perovskite device, solution process methods are widely employed and thus, these are discussed in detail.

5.3.2. One-step and two-step solution based methods

The chemical based routes are liquid and gas phases based and in the development of perovskite solar cell devices, as stated solution process method is undertaken employing spin coating or dip coating. In these devices, typically absorber and transport layers are developed so far as per device architecture and willingness in order to achieve desired PCE and stability with cost effectiveness. The solution process is classified as one and two step solution based methods.

5.3.2.1. One-step solution-based method. In the one-step solution-based method which is pictorially represented in Fig. 11, the desired compositions of the materials viz. CH₃NH₃I and PbI₂ (particularly for the CH₃NH₃PbI₃ perovskites) is chosen and a solution is prepared using an appropriate solvent like chlorobenzene, dichloromethane, diethyl ether, toluene, isopropanol (IPA) etc. This solution is coated on the substrate comprising of transport layer followed by the heat treatment of the deposited perovskite layer (Xu et al., 2015; Ahn et al., 2015).

Im and others (Im et al., 2011) prepared perovskite absorber layer via one-step approach where, the CH₃NH₃I and PbI₂ (1:1) compounds were dissolved in γ -butyrolactone (GBL) and stirred for 12 h at 60 °C and the prepared solution was then filtered using Polyvinylidene Fluoride (PVDF) filter. They varied the annealing temperatures as 40 °C, 60 °C and 100 °C and observed that as compared to the pristine samples, the annealed ones showed better PCE. An impact of annealing temperature on the one step-spin coated perovskite absorber layer was reported (Dualeh et al., 2014). For the annealing temperatures ranging within 60–200 °C, the perovskite films were not showed any change in color while later, on annealing these above 200 °C, color of these changed into yellow indicated degradation by decomposing into CH₃NH₃I and PbI₂. This technique was employed to prepare perovskite absorber layer (Ahn et al., 2015) where MAI, PbI₂ and Dimethylsulfoxide (DMSO) (1:1:1) were dissolved in Dimethylformamide (DMF) and diethyl ether solvents and devices attained PCE of 19.7 %. An impact of solvents on surface morphology of perovskite absorber was investigated by applying one-step approach (Kim et al., 2014c) where three different solvents, DMF, GBL and DMF:GBL (97:3) were used to attain compact and interconnected morphology for the perovskite layers and by incorporating these perovskite absorbers in the PSCs resulted into PCE of more than 6 %. Sometimes excess PbI₂ might be resulted to pretty performance of the devices and accordingly, devices comprised of one-step solution based excess PbI₂ absorber layer attained higher PCE of 19 % (Carmona et al., 2015).

5.3.2.2. Two-step solution-based method. Two-step solution-based method can be implemented via two pathways where in first, solutions of CH₃NH₃I and PbI₂, particularly for the CH₃NH₃PbI₃ perovskite, is prepared and deposited sequentially using spin coating technique and after that, the deposited layer is subjected to thermal annealing for proper conversion of both the compounds into CH₃NH₃PbI₃ perovskite absorber. In the second pathway firstly, the prepared PbI₂ solution is deposited on transport layer embraced substrate by spin coating technique and then dipped it into CH₃NH₃I solution followed by subjecting the deposited perovskite layer to heat treatment. The lack of reproducibility and lesser control over uniformity of the developed layers are disadvantages of the two-step solution-based method and therefore, one-step solution-based method is typically preferred for fabrication of perovskite layers in solar cell device (Liu et al., 2013; Baker et al., 2013). A graphical view of two-step solution method is depicted in Fig. 12.

In perovskite solar cell devices, variation in constituent elements to

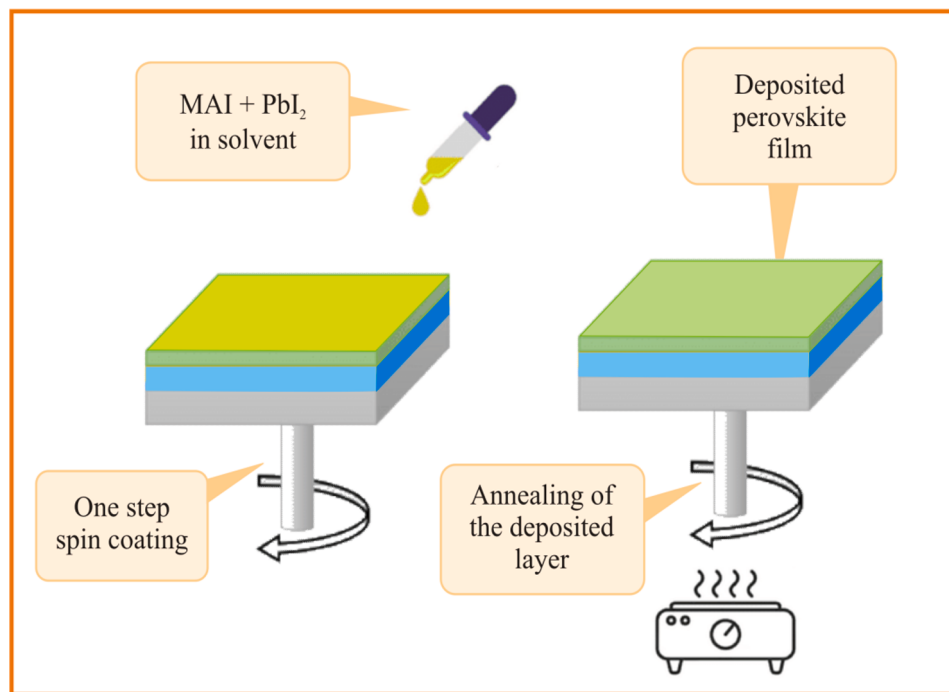


Fig. 11. Representation of one step solution-based method for developing $\text{CH}_3\text{NH}_3\text{PbI}_3$ perovskite absorbers.

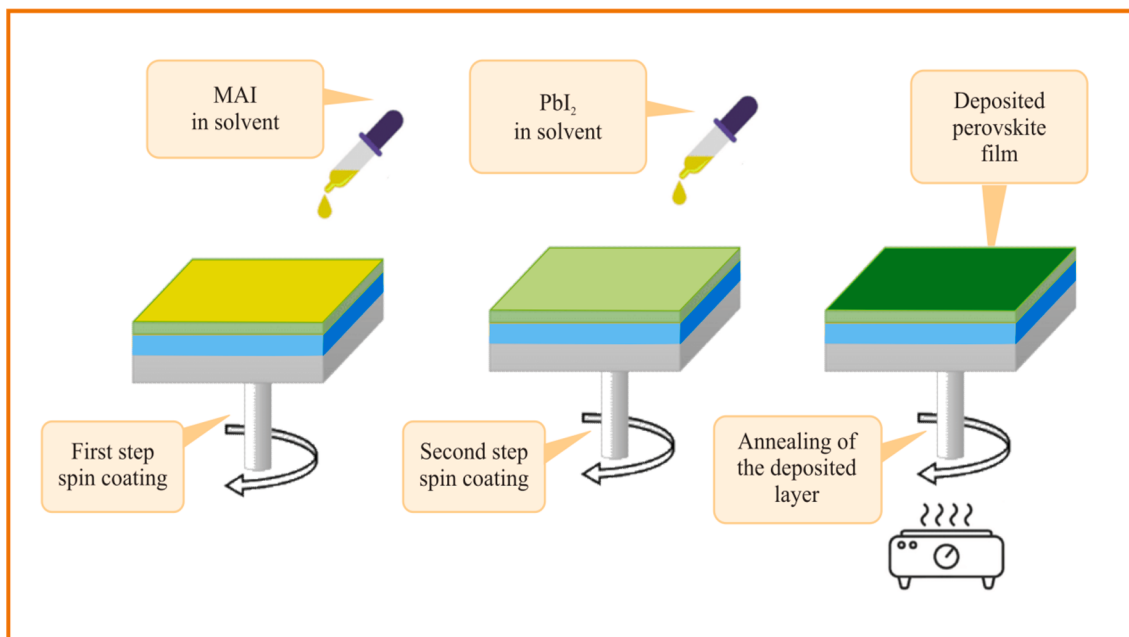


Fig. 12. Graphical view of two-step solution-based method for developing $\text{CH}_3\text{NH}_3\text{PbI}_3$ absorber layers.

perovskite material alters properties of the absorber layer which ultimately affect the device performance and therefore, next section deals with compositional engineering to PSCs and its impact on the PCE and stability.

6. Compositional engineering to perovskite solar cells

As stated, the stability and PCE of perovskite solar cells are also affected by varying typical composition (ABX_3) of perovskite structure. An impact of compositional variation on stability and PCE have been reported so far where three kinds of variations could be made in

monovalent cation (A), divalent cation (B) and halide or anion (X) and details on the variations along with impact on properties and performance is provided in following sub-sections.

6.1. Monovalent cation replacement

In perovskite absorbers, the monovalent cation, Methylammonium (MA^+) has been replaced so far by Formamidinium (FA^+), Cesium (Cs^+), Ethylammonium (EA^+) and Butylammonium (BA^+) where FA^+ and Cs^+ are mostly used. The replacement of MA^+ by FA^+ can lead to better electrical properties, higher symmetry and PCE but, it lowers the band

gap of perovskite absorbers (Pellet et al., 2014). In a replacement work of MA^+ by FA^+ (Kumari et al., 2019), the higher PCE of 12.81 % was attained for FAPbI_3 as compared to 7.39 % for MAPbI_3 under similar conditions. The effect of replacing MA^+ by Cs^+ on the PCE and stability of PSCs was undertaken (Aamir et al., 2018) where findings revealed that although CsPbI_3 devices have better thermal stability under ambient conditions yet with lower PCE as compared to MA devices which might be due to attaining structure and phase change of Cs^+ cation into orthorhombic at room temperature. Similarly, replacing MA^+ cations by large-sized cations like EA^+ or BA^+ also led to the formation of orthorhombic phased structure which increased the band gap of perovskite layers (>2 eV) (Zhang et al., 2019). In order to attain higher PCE and stability, the perovskite devices are also developed by hybrid or mixed cation and accordingly, hybrid cation $\text{MA}_x\text{FA}_{1-x}\text{PbI}_3$ absorbers were applied by altering MA and FA compositions and as a result, energy band gap to perovskite absorbers was tailored by achieving higher PCE of 14.9 % for composition $\text{MA}_{0.6}\text{FA}_{0.4}\text{PbI}_3$. Zhang and others (Zhang et al., 2018) have reported perovskite devices comprising of hybrid cations and achieved 16.84 % PCE with enhanced stability of more than 180 days. The varying Cs^+ cation composition ($\text{Cs}_x(\text{MA}_{0.17}\text{FA}_{0.83})_{100-x}\text{Pb}(\text{I}_{0.83}\text{Br}_{0.17})_3$) perovskite devices (Saliba et al., 2016) demonstrated increased stability with desired PCE of 21.1 %.

6.2. Divalent cation replacement

In perovskite absorbers, as divalent cation, lead (Pb^{2+}) is widely used due to its high stability and PCE but owing to its lethal nature, non-toxic and eco-friendly replacements are required and thus, Pb^{2+} is replaced either by Tin (Sn^{2+}) or Germanium (Ge^{2+}) (Liu et al., 2016). The MASnI_3 and MAPbI_3 perovskites were studied using the theoretical approach (GW calculation method) (Umari et al., 2014) and *ab-initio* density functional theory (DFT) (Tao et al., 2017) and predicted that MASnI_3 perovskites could have better charge carrier transportation and optical properties vis-a-vis to MAPbI_3 and thus, MASnI_3 could be desirable for Lead free solar cell devices. Although both the Sn and Ge are eco-friendly yet these have limitations under ambient conditions as Sn^{2+} gets easily oxidized to Sn^{4+} and Ge is rarely applied owing to its erratic nature in the +2 oxidation state (Nair et al., 2020). The higher PCE could be attained using the mixed/hybrid divalent cations in perovskite devices (Kumari et al., 2019; Kumari et al., 2018c) and accordingly, mixed divalent cation $\text{FAPb}_{0.5}\text{Sn}_{0.5}\text{I}_3$ perovskite absorber embraced devices attained higher PCE of 14.09 % as compared to 12.81 % for FAPbI_3 devices (Kumari et al., 2019). In another work, hybrid $\text{CH}_3\text{NH}_3\text{Pb}_{0.5}\text{Sn}_{0.5}\text{ICl}_2$ and $\text{CH}_3\text{NH}_3\text{Pb}_{0.5}\text{Sn}_{0.5}\text{I}_3$ perovskite absorber comprised devices acquired higher PCE of 10.20 % and 10.61 %, respectively whereas devices without Sn exhibited lower PCE of 7.39 % (Kumari et al., 2018c).

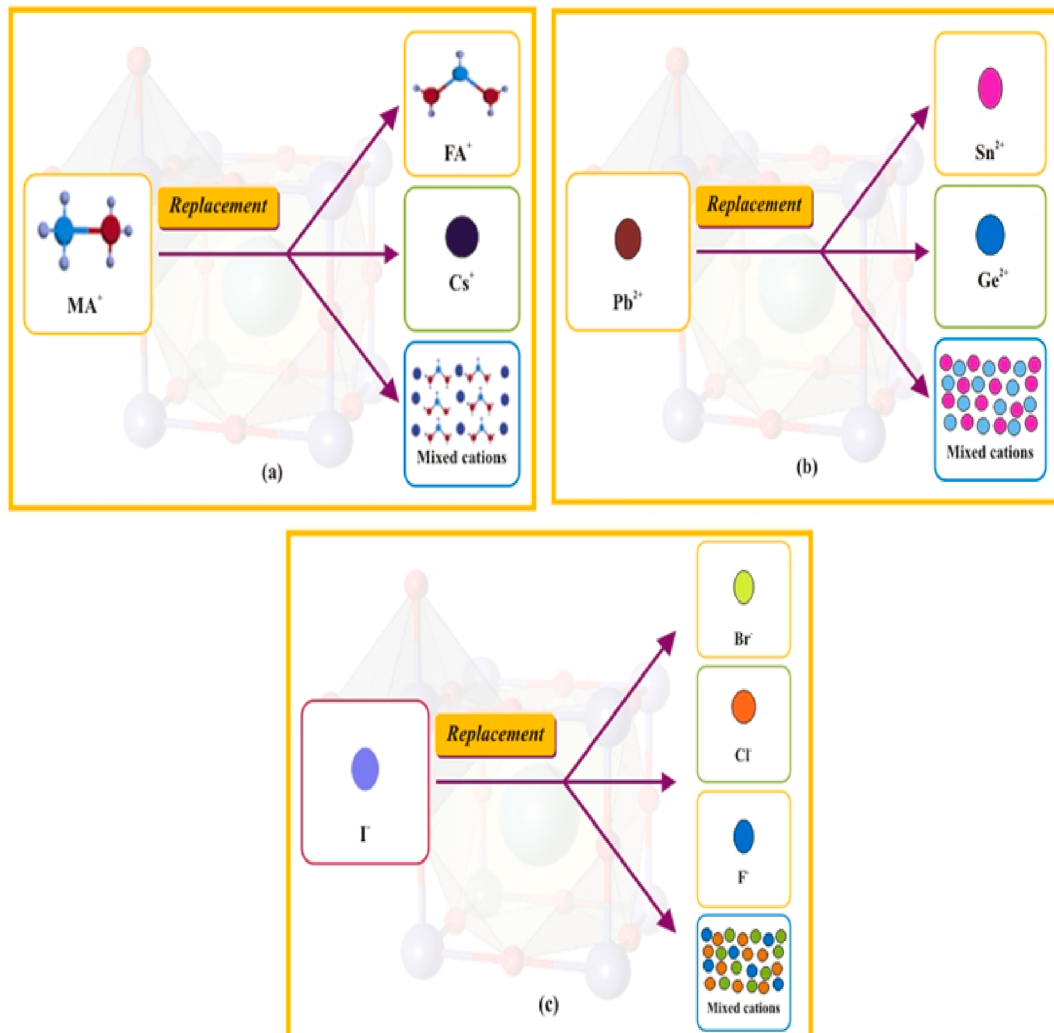


Fig. 13. Pictorial representation of compositional replacement for (a) monovalent cation (A), (b) divalent cation (B) and (c) anion (X) in perovskite solar cells.

6.3. Anion/halide replacement

The Iodine (I^-) is usually preferred in the perovskite absorbers and has closer electro negativity to Lead (Pb) however, I^- can be replaced by Bromine (Br^-), Chlorine (Cl^-) and Fluorine (F^-). A pictorial representation of compositional replacements is depicted in Fig. 13.

Both the Br^- and Cl^- possess cubic structure under ambient conditions which is suggestive of good stability but, the crystals of Br^- are larger in size causing lattice distortion leading to lesser PCE. Also using Cl^- , the charge carrier lifetime and diffusion length could be improved, but Cl^- precursor has lesser miscibility (Ansari et al., 2018). Due to these drawbacks of Bromine (Br^-) and Chlorine (Cl^-), the use of mixed halide perovskite absorbers in the device concerned is undertaken (Noh et al., 2013a; Lee et al., 2012). The varying Br composition ($CH_3NH_3Pb(I_{1-x}Br_x)_3$) absorber based devices demonstrated higher PCE of 12.3 % for $x = 0.2$ with stability too (Noh et al., 2013a). The mixed halide $CH_3NH_3PbI_2Cl$ based devices showed PCE of 10.9 % with higher stability (Lee et al., 2012). Nonetheless, the current research trends are suggestive of the facts that alterations in composition/compositional engineering to the perovskite absorbers must be optimized properly in order to achieve higher PCE with stability. A schematic illustration summarizing the compositional variation in PSCs is portrayed in Fig. 14.

The PCE and stability in PSCs are typically affected by environmental conditions which are dealing with degradation of the devices and thus, following section aptly explains these factors along with the possible solutions.

7. Factors affecting the performance of perovskite solar cells and possible solutions

Perovskite solar cells have gained tremendous attention due to their desirable properties, but still the lifetime of PSCs i.e. the shelf life or life span determining up to how long a perovskite solar cell can last/survive is still an issue, since Silicon solar cells have lifetime of 25 years whereas the PSCs can last only upto a year. A two dimensional bar diagram comprising the lifetime of Silicon and perovskite solar cells is shown in Fig. 15.

There are so many factors those affect the stability of the PSCs such as thermal instability, moisture and Oxygen, toxicity, electrical biasing, additives, interfaces and illumination. These factors and the possible solutions concerned are described in detail herein.

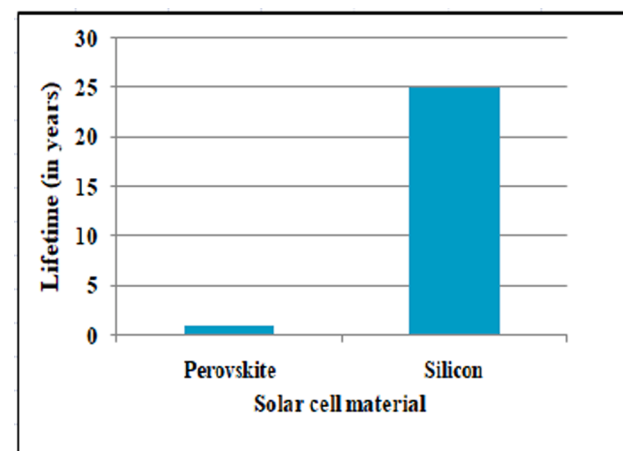


Fig. 15. 2D bar diagram comparing the lifetime of perovskite and Silicon solar cells.

7.1. Thermal instability in the perovskite solar cells

The thermal treatment is typically necessary step not only for the thin film devices but for the PSCs too as it improves the physical properties to the devices but, it may also cause instability by degrading perovskite absorber in the device. The issue of thermal instability in perovskite devices is highlighted so far in literature (Misra et al., 2015; Conings et al., 2015). The work focused on thermal stability in $MAPbI_3$ perovskite devices demonstrated stability at room temperature and but for the elevated temperatures within 45–55 °C range, $MAPbI_3$ absorber was found to be decomposed into its components (Misra et al., 2015) which was also followed by Coining et al. (Conings et al., 2015) who reported $MAPbI_3$ perovskite layer decomposition into PbI_2 and MAI at 85 °C. In all these works, the decomposition of absorber is happened during the device development. The replacement of MA cation by FA provided thermal stability which was assured in a study where $MAPbI_3$ and $FAPbI_3$ perovskite absorbers were thermally annealed at 150 °C. As a consequence, $MAPbI_3$ decomposed into its components whereas $FAPbI_3$ successfully withstand this temperature without discoloration (Eperon et al., 2014b).

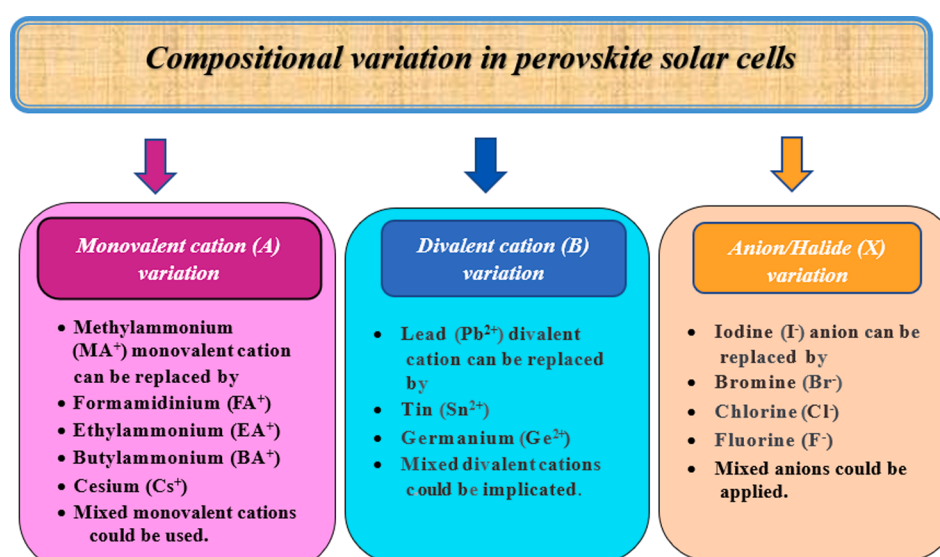


Fig. 14. Schematic representation summarizing compositional variation in PSCs.

7.2. Moisture and Oxygen driven degradation

The perovskite absorbers to the PSC devices are typically degraded when come in contact with humidity and Oxygen which caused instability in the device concerned (Naghadeh et al., 2018). As explained in section 4.2 by chemical reactions, a 4-step breakdown mechanism to $\text{CH}_3\text{NH}_3\text{PbI}_3$ perovskite absorber on interacting with moisture and Oxygen demonstrated its degradation into $\text{CH}_3\text{NH}_3\text{I}$ and PbI_2 by changing color from dark brown to light yellow. On using a material comprising of hydrophobic nature in perovskite devices and this property could help to tackle degradation problem owing to moisture and this process is typically called hydrophobic passivation. The hydrophobic passivation was employed by spin coating a Polytetrafluoroethylene (PTFE) layer on top of the device resulted into negligible decomposition upto 30 days (Hwang et al., 2015). The degradation could also be prevented by an additional layer of Al_2O_3 between perovskite absorber and HTL (Qiu et al., 2020). Also sometimes Oxygen from the atmosphere is not responsible for degradation of the device but, Oxygen ions from the ETL like TiO_2 could also responsible for the device degradation. Employing the compositional engineering especially to the absorber, oxidation effect in devices could be minimized to reduce degradation (Chen et al., 2017).

7.3. Toxicity of Lead-based perovskite solar cells

The Lead (Pb) is widely used for fabrication of perovskite solar cell devices but, fatal nature of Lead is a major concern. It can be avoided in two ways either by minimizing Lead content or by completely replacing Lead from the PSC devices while the main drawback in reducing Lead composition or Lead free devices, these would exhibit lower PCE. The Sn-based mixed/hybrid inverted planar devices exhibited better stability and charge collection with lower recombination rate as revealed by a reported work comprising of 9 % PCE (Shao et al., 2018). The inorganic KBaTeBiO_6 perovskite absorber incorporated PSC devices predicted better charge transport and optical properties employing linear regression analysis and DFT but, the workers are not able to validate the findings experimentally as the obtained experimental PCE was only 0.057 % (Thind et al., 2019). An impact of Lead free, inorganic Cs_2TiBr_6 perovskite based planar FTO/ZnO/ Cs_2TiBr_6 / MoO_3 /Au device employing SCAPS-1D simulation program predicted PCE of 18.15 % (Khan et al., 2021). On applying cost effective Carbon (C) as back contact resulted into PCE of 18.11 % which is comparable to the earlier. Similar to the thin film solar cells, the perovskite devices are embraced several thin film constituent layers which are comprised of grain boundaries those behave like trap states and recombination centers for the generated charge carriers, ultimately reduce performance of a device. Such simulation codes do not comprise impact of grain boundaries and as a consequence, validation of the theoretical findings with the experiments is a challenging task.

7.4. Bias-dependent degradation of perovskite solar cells

In a solar cell device, without an external electrical field, the potential difference developed across the junction in equilibrium condition is termed as build-in-potential. Usually organic and inorganic perovskite absorbers have low ion mobilities, while under electrical biasing of the device, ion mobility increases and ions are migrated speedily towards interface between perovskite layer and electrodes owing to non-equilibrium condition and developed built-in-potential. The charge accumulation at the interface would be responsible for defects generation which ultimately affect performance of the devices (Roy et al., 2020; Tress et al., 2015). A study on degradation of PSCs under electrical biasing condition demonstrated that faster degradation of the PSC took place under open circuit (OC) conditions owing to the trapping of charge carriers and unwanted extrinsic ion diffusion while short circuit (SC) and maximum power point (MPP) conditions led to slower degradation

(Khenkin et al., 2019). The electric field induced ion defect migration along with its impact on long-term performance of PSCs is reported (Domanski et al., 2017) where anion vacancies are migrated and collected at interface dealing with hole selective contact. This accretion has been increased on shifting the biasing from forward to reverse. Also, accumulation of cation vacancies corresponding to the electric field induces reversible losses in the device performance. On keeping the device in dark for longer period, the PCE is entirely recovered or every morning, device showed PCE similar to that of the freshly fabricated PSCs. Day-night cycling also affect biasing and degradation mechanism. An impact of cycling test on $\text{CH}_3\text{NH}_3\text{PbI}_3$ devices was reported by taking 12 hrs cycling corresponding to illumination and dark conditions and observed fatigue behavior with diurnal cycling. In dark condition for 12 h, PCE was reduced lesser than 10 % of its maximum value which was restored gradually after keeping device few hours under illumination. However, the overall performance of the device was decreased with each consecutive illumination/darkness cycles which validated the fatigue behavior (Huang et al., 2016).

A degradation experiments was performed on Glass/ITO/TiO₂/CH₃NH₃PbI₃/SpiroOMeTAD/Au and Glass/ITO/SnO₂/Cs_{0.05}((CH₃NH₃)_{0.15}(CH(NH₂)₂)_{0.85})_{0.95}PbI_{2.55}Br_{0.45}/SpiroOMeTAD)/Au devices by observing involvement of a number of irreversible and reversible processes in device degradation under electrical biasing conditions. Instead of T₈₀ which is defined as the time when power conversion efficiency decreases to 80 % of its initial value and initial PCE, the energy output produced during the first day of light exposure has been used. The obtained diurnal PCE variation was reversible and stability testing along with light/dark cycling of the PSC devices is important too (Khenkin et al., 2018). Also, a study on degradation with electrical biasing conditions along with recovery of ITO/SnO₂/Cs_{0.15}(CH-(NH₂)₂)_{0.85}PbI_{2.7}Br_{0.3}/SpiroOMeTAD/Au devices revealed a reduction in device PCE under illumination upto 60 % or 80 % of the initial value those are termed as T₆₀ or T₈₀. The devices were recovered by operating under open and short circuit conditions with electrical biasing (Prete et al., 2021). The International Summit on Organic Photovoltaic Stability (ISOS) protocols demonstrated stability testing for organic photovoltaics (OPVs) corresponding to PSC devices features like analyzing intrinsic solar cell stability (I), light-dark cycling (ISOS-LC) imitating the diurnal cycle and solar cell behavior under electrical biasing conditions and under dark condition (ISOS-V) (Khenkin et al., 2020).

7.5. Role of additives in the perovskite solar cells

The additives plays crucial role in altering PCE and stability of the PSC devices. Additives like polymers (Polyethylene Glycol (PEG)), Tetra-ammonium Zinc Phthalocyanine (ZnPc), bidentate (Bpy) and tri-dentate (Tpy)), fullerene (PC₇₀BM, ICBA, ThCBM, PC₇₁BM and PC₆₁BM), and organic/inorganic halide salts (Li-TFSI) have been widely used so far in precursor solutions (Li et al., 2017). Amongst the all, polymers are believed to have good solubility in the solvents and accordingly, MAPbI₃ devices were fabricated by adding PEG in PbI₂ and MAI solutions (Zhao et al., 2016) which made the device moisture resistant along with better PCE of 16 %. Guo and coworkers (Guo et al., 2016) incorporated polymer polyvinylpyrrolidone (PVP) additive in precursor solution of MAI, PbI₂ and PbCl₂ for the fabrication of hybrid CH₃NH₃PbI_{3-x}Cl_x based devices and attained 7.34 % PCE along with thermal stability and also prevented the devices from getting deterioration.

7.6. Role of interfaces/contacts in the perovskite solar cells

The interfaces/contacts between absorber layer and charge transport layers (ETLs and HTLs) play an important role in proper charge collection along with improving performance of perovskite solar cell device. Due to the hydrophilic nature, the perovskite absorbers can absorb moisture from surroundings and as a consequence, the absorber layer is

degraded into its constituents by creating defects at the ETL/perovskite and perovskite/HTL interfaces. These defects act as charge recombination sites where the charge carriers could be trapped. In order to tackle this issue, a buffer layer of materials like Al_2O_3 could be inserted between the absorber and charge transport layers (Qiu et al., 2020).

7.7. Degradation of perovskite solar cells under illumination

The perovskite devices are degraded when exposed under illumination (Niu et al., 2015; Snaith, 2013; Chander et al., 2014; Fujishima et al., 2000; Joshi et al., 2016) which is called photo-induced degradation. As depicted earlier, although several modifications are made in transport layer to the PSC devices yet typically TiO_2 is applied as ETL which could be degraded under UV illumination. The degradation mechanism under UV illumination can be explained by Eqs. (9)–(11) where electrons are extracted from the TiO_2 layer, break perovskite structure and form I^- ions followed by I_2 formation. On interaction with the UV photons, the desorbed Oxygen released from the vacant and trap sites are got activated which increased charge carriers recombination and as a result, it reduces device performance by decreasing FF and V_{oc} concerned.



The titania ETL layer could be protected from getting degradation by implicating modifications and as per available literature, two methods could be adopted viz. (a) complete removal of the titania layer from the fabricated PSCs and (b) prevent the titania layer surface from exposing through UV irradiance by suitable encapsulation (Chander et al., 2014). A pictorial representation of the factors affecting the PSCs performance is depicted in Fig. 16 which are also tabulated in Table 3 along with solutions to mitigate the problems.

In order to attain higher stability and PCE and to lessen degradation

Table 3
The factors which affect PSC device performance along with their solutions.

Factors	Solutions	Ref.
Thermal instability	• By replacing cation MA by FA.	(Eperon et al., 2014b)
Moisture and Oxygen	• By using hydrophobic HTLs. • By applying additional layer between absorber and HTL.	(Hwang et al., 2015; Qiu et al., 2020)
Toxicity	• By replacing Pb by Sn or Ge. • By reducing Lead content or Lead free structure.	(Shao et al., 2018; Thind et al., 2019; Khan et al., 2021)
Electrical Biasing	• Proper optimization of charge extraction and diurnal cycles.	(Khenkin et al., 2019)
Additives	• By using polymers with good solubility in precursors.	(Zhao et al., 2016; Guo et al., 2016)
Interfaces	• By inserting buffer layer between perovskite and charge transport layers.	(Qiu et al., 2020)
Illumination	• Proper encapsulation of titania ETL.	(Chander et al., 2014)

probability in these devices, one dimensional (1-D), two dimensional (2-D) and three dimensional (3-D) perovskite absorbers could be implemented (Gao et al., 2019; Zuo et al., 2019). The next section comprises a brief description on the commercialization strategy to the perovskite solar cell devices.

8. Commercialization grade of perovskite solar cells

In solar cell devices, three factors decide their commercialization viz. (a) stability (b) cost and (c) performance of the device. The development in fabrication techniques and device structure could bring these devices effectively in the society with commercialization at the next level instead of confining these only at the laboratory scale. Although these devices offer performance with cost effectiveness yet stability is a crucial issue that need to be tackled efficiently (Roy et al., 2020). The commercialization at large scale along with higher PCE and stability

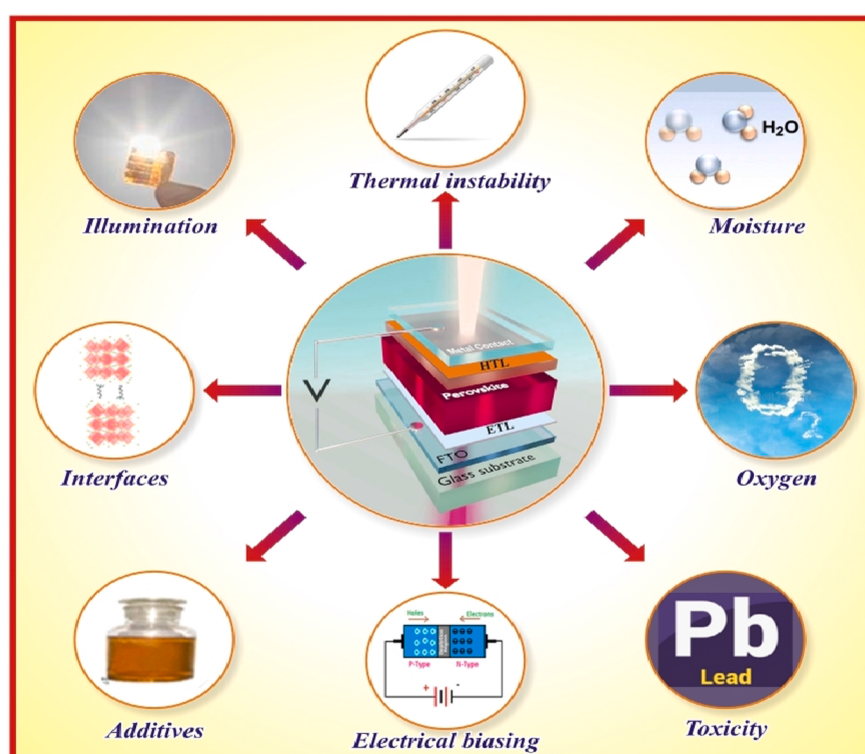


Fig. 16. Schematic illustration of the factors which affect PSC device performance.

Table 4

The IEC 61215 standard protocols along with module parameters.

Test	Role	Parameters	Ref.
Thermal cycling test	• To determine ability of a solar cell module to resist fatigue, thermal mismatch and other stresses.	• Maximum cycling time: 6 hours. • Minimum dwelling time: 10 minutes. • Thermal cycling temperature range: –40 °C to 85 °C. • Cooling or heating rate: 100 °C per hour for maximum 200 cycles.	(Roy et al., 2020; Nair et al., 2020)
Damp heat test	• To determine ability of a solar cell module to withstand the adverse effects of long term penetration of moisture.	• Test duration: 1000 hours. • Relative humidity (RH): 85 % ± 5 %.	(Nair et al., 2020; Lee and Park, 2020; Holzhey and Saliba, 2018)
Humidity-freeze test	• To determine ability of a solar cell module for enduring the adverse effects of moisture and high temperatures.	• Rapid freezing temperature range: 0 °C to –40 °C. • Maintenance temperature: –40 °C for 4 hours maximum 10 cycles	(Nair et al., 2020; Lee and Park, 2020; Holzhey and Saliba, 2018)

need to pass industry standards through International Electrochemical Commissions (IEC) tests as per IEC 61215 protocols. The long term stability and device performance to the developed PV module could be justified by these protocols and then, one can attain confidence of the market and industry leading to up-liftment in commercialization of PV modules (Roy et al., 2020; Nair et al., 2020). For stability, these tests are classified into three categories as (a) Thermal cycling test (b) Damp heat test and (c) Humidity-freeze test (Lee and Park, 2020; Holzhey and Saliba, 2018; IEC 61215, 2016; Cheacharoen et al., 2018) which are also depicted in tabular form in Table 4. Earlier, the IEC PV test standards were set only for the crystalline solar cells. Later on, these are followed by amendments in standards to include thin film devices as well. In present, these tests have been applied for the CdTe, CIGS and perovskite devices.

In uplifting the commercialization grade to PSC devices, a number of companies across the globe have played their important role and accordingly, Microquanta, a semiconductor-based company of China, fabricated PSCs on mini-modules by attaining PCE of 17.4 % (Peleg, 2018). In 2016, a Switzerland based company named Solaronix achieved 12 % PCE to the PSC modules for an effective device area of 500 cm² (Solaronix Achieves Major Breakthrough Toward Perovskite Solar Cell Industrialization, 2016) followed by 14 % for monolithic perovskite modules with lifetime of 10,000 h (Hashmi et al., 2017) in 2017. The Oxford PV developed perovskite devices with champion Si devices for Si/perovskite tandems and achieved record breaking PCE of 28 % in 2018 with device effective area of 1 cm² by passing 2000 h damp heat test for compelling justification of the reliability as per IEC 61215 protocol (Oxford PV perovskite solar cell achieves 28% efficiency, 2018).

As stated, a thin film solar cell device comprises several constituent layers which embrace huge grain boundaries those affect not only the film properties but the device performance too as normal and parallel alignments of these boundaries affect the charge carrier flow differently. Thus, the device design and simulation modeling algorithm should be comprised of impact of grain boundaries dealing with constituent layers to the PSC devices while, the codes reported so far are away from this incorporation.

9. Conclusion and future scope

The perovskite solar cell devices have emerged tremendously and demonstrated amazing power conversion efficiency during last one decade at laboratory scale but still need to take a colossal leap in terms of the PV module performance. Although the perovskite absorbers to the PSC devices have greater optoelectronic properties like high absorption coefficient, optimum tunable band gap, high electron and hole mobilities, excellent charge transport properties yet lacking Silicon PV devices which are still champion not only at the laboratory scale but industry too along with stability concerns. This review efficiently dealt with recent research development and issues of the PSC devices in terms of stability and PCE. It depicted brief history for the perovskite materials and devices concerned along with the chemical and structural aspects. Two most commonly used device architectures have been discussed along with materials evolution to the ETL, HTL and perovskite absorbers as well as implication of organic and inorganic materials as ETL and HTL. Two manufacturing routes applied so far for fabrication the perovskite absorbers have been discussed with compositional engineering to the perovskite absorbers. The degradation mechanism in PSC devices under various environmental conditions is deliberated in light of limited literature along with possible solutions for the further improvement. The commercialization status and strategy of the PSCs are described too in terms of the IEC61215 norms and protocols. Undoubtedly PSC devices have shown admirable PV performance during this decade while stability is still an issue which needs to be resolved along with maintaining cost effectiveness and PCE. The materials evolution for the constituent layers should be done along with desired device design by employing a suitable simulation modeling algorithm comprising of impact of grain boundaries exist in the thin film constituent layers to the PSC device. Though the authors have tried to incorporate the available relevant literature so far but, they have apology to not to include, if any transaction has been left inadvertently.

Declaration of Competing Interest

The authors declare that they have no known competing financial interests or personal relationships that could have appeared to influence the review presented in this paper.

Acknowledgment

The authors sincerely acknowledge the Ministry of Education, Government of India and Ministry of Higher Education, Government of Rajasthan, India for financial assistance through RUSA 2.0, Research and Innovation project to Dr. M.S. Dhaka (Principal Investigator) and Dr. Shikha Agarwal (Co-Investigator). One of us, Arushi Sharma is thankful to University Grants Commission (UGC), New Delhi, India for Junior Research Fellowship (JRF) vide number 191620056397.

References

- Aamir, M., Adhikari, T., Sher, M., Revaprasadu, N., Khalid, W., Akhtar, J., Nunzi, J.M., 2018. New J. Chem. 42, 14104–14110.
- Ahn, N., Son, D.Y., Jang, I.H., Kang, S.M., Choi, M., Park, N.G., 2015. J. Am. Chem. Soc. 137, 8696–8699.
- Aitola, K., Sveinbjörnsson, K., Baena, J.P.C., Kaskela, A., Abate, A., Tian, Y., Johansson, E.M.J., Gratzel, M., Kauppinen, E.I., Hagfeldt, A., Boschloo, G., 2016. Energy Environ. Sci. 9, 461–466. <https://doi.org/10.1039/C5EE03394B>.
- Al-Ashouri, A., Köhnen, E., Li, B., Magomedov, A., Hempel, H., Caprioglio, P., Márquez, J.A., Morales Vilches, A.B., Kasparavicius, E., Smith, J.A., Phung, N., Menzel, D., Grischek, M., Kegelmann, L., Skroblin, D., Gollwitzer, C., Malinauskas, T., Jošt, M., Matić, G., Rech, B., Schlatmann, R., Topič, M., Korte, L., Abate, A., Stannowski, B., Neher, D., Stolterfoht, M., Unold, T., Getautis, V., Albrecht, S., 2020. Science 370, 1300–1309.

- Ansari, M.I.H., Qurashi, A., Nazeeruddin, M.K., 2018. *J. Photochem. Photobiol. C* 35, 1–24.
- Ashgar, M.I., Zhang, J., Wang, H., Lund, P.D., 2017. *Renew. Sustain. Energy Rev.* 77, 131–146.
- Baena, J.P.C., Abate, A., Saliba, M., Tress, W., Jacobsson, T.J., Gratzel, M., Hagfeldt, A., 2017b. *Energy Environ. Sci.* 10, 710–727.
- Baena, J.P.C., Saliba, M., Buonassisi, T., Gratzel, M., Abate, A., Tress, W., Hagfeldt, A., 2017a. *Science* 358, 739–744.
- Bailie, C.D., Christoforo, M.G., Mailoa, J.P., Bowring, A.R., Unger, E.L., Nguyen, W.H., Burschka, J., Pellet, N., Lee, J.Z., Gratzel, M., Noufi, R., Buonassisi, T., Salleo, A., McGehee, M.D., 2015. *Energy Environ. Sci.* 8, 956–963. <https://doi.org/10.1039/C4EE03322A>.
- Baker, R.H., Nazeeruddin, M.K., Burschka, J., Gao, P., Pellet, N., Gratzel, M., Moon, S.J., 2013. *Nature* 499, 316–319.
- Bakr, Z.H., Wali, Q., Fakharuddin, A., Mende, L.S., Brown, T.M., Jose, R., 2017. *Nano Energy* 34, 271–305.
- Bartel, C.J., Sutton, C., Goldsmith, B.R., Ouyang, R., Musgrave, C.B., Ghiringhelli, L.M., Scheffler, M., 2019. *Sci. Adv.* 5 (2), 1–9.
- Becquerel, A.E., 1839. *C. R. Acad. Sci. I*, 9, 561.
- Berhe, T.A., Su, W.N., Chen, C.H., Pan, C.J., Cheng, J.H., Chen, H.M., Tsai, M.C., Chen, L.Y., Dubale, A.A., Hwang, B.J., 2016. *Energy Environ. Sci.* 9 (2), 323–356. <https://doi.org/10.1039/C5EE02733K>.
- Bi, D., Yi, C., Luo, J., Déköppet, J.D., Zhang, F., Zakeeruddin, S.M., Li, X., Hagfeldt, A., Grätzel, M., 2016. *Nat. Energy* 1(10), 1–5. DOI: <https://doi.org/10.1038/energy.2016.142>.
- Bowman, A.R., Lang, F., Chiang, Y.H., Jiménez-Solano, A., Frohma, K., Eperon, G.E., Ruggeri, E., Abdi-Jalebi, M., Anaya, M., Lotsch, B.V., Stranks, S.D., 2021. *ACS Energy Lett.* 6, 612–620.
- Burschka, J., Pellet, N., Moon, S.J., Baker, R.H., Gao, P., Nazeeruddin, M.K., Grätzel, M., 2013. *Nature* 499 (7458), 316–319.
- Bush, K.A., Palmstrom, A.F., Yu, Z.J., Boccard, M., Cheacharoen, R., Mailoa, J.P., 2017. *Nat. Energy* 2, 17009.
- Cao, Y., Gao, F., Xiang, L., Li, H., Li, D., Liu, Q., Liu, H., Zou, C., Li, S., 2022. *Adv. Mater. Interfaces* 9 (21), 2200179.
- Cao, X., Zhi, L., Jia, Y., Li, Y., Zhao, K., Cui, X., Ci, L., Zhuang, D., Wei, J., 2019. *ACS Appl. Mater. Interfaces* 11 (8), 7639–7654.
- Carmona, C.R., Gratia, P., Zimmermann, I., Grancini, G., Gao, P., Graetzel, M., Nazeeruddin, M.K., 2015. *Energy Environ. Sci.* 8, 3550–3556.
- Chander, N., Khan, A.F., Chandrasekhar, P.S., Thouti, E., Swami, S.K., Dutta, V., Komarala, V.K., 2014. *Appl. Phys. Lett.* 105, 033904 <https://doi.org/10.1063/1.48991181>.
- Cheacharoen, R., Rolston, N., Harwood, D., Bush, K.A., Dauskardt, R.H., McGehee, M.D., 2018. *Energy Environ. Sci.* 11, 144–150. <https://doi.org/10.1039/C7EE02564E>.
- Chen, J., Seo, J.Y., Park, N.G., 2018. *Adv. Energy Mater.* 8, 1702714.
- Chen, W., Xu, L., Feng, X., Jie, J., He, Z., 2017. *Adv. Mater.* 29, 1603923.
- Chen, P.Y., Yang, S.H., 2016. *Opt. Mater. Express* 6 (11), 3651–3669.
- Chen, Q., Zhou, H., Hong, Z., Luo, S., Duan, H., Wang, H., Liu, Y., Li, G., Yang, Y., 2014. *J. Am. Chem. Soc.* 136 (2), 622–625.
- Chiang, C.H., Tseng, Z.L., Wu, C.G., 2014. *J. Mater. Chem. A* 2, 15897–15903.
- Cho, A.N., Park, N.G., 2017. *Chem. Sustain. Energy Mater.* 10, 3687–3704.
- Christians, J.A., Fung, R.C.M., Kamat, P.V., 2014. *J. Am. Chem. Soc.* 136, 758–764.
- Ciro, J., Betancur, R., Mesa, S., Jaramillo, F., 2017. *Sol. Energy Mater. Sol. Cells* 163, 38–42.
- Conings, B., Drijkoningen, J., Gauquelain, N., Babayigit, A., Haen, J.D., Olieslaeger, L.D., Ethirajan, A., Verbeeck, J., Manca, J., Mosconi, E., Angelis, F.D., Boyen, H.G., 2015. *Adv. Energy Mater.* 5 (15), 1500477. <https://doi.org/10.1002/aenm.201500477>.
- Czochralski, J., 1918. *Z. Phys. Chem.* 92, 219–221.
- Denegri, G.M., Colodrero, S., Kramarenko, M., Martorell, J., 2018. *ACS Appl. Energy Mater.* 1 (10), 5548–5556. <https://doi.org/10.1021/acsaem.8b01118>.
- Djurisic, A.B., Liu, F.Z., Tam, H.W., Wong, M.K., Ng, A., Surya, C., Chen, W., He, Z.B., 2017. *Prog. Quantum Electron.* 53, 1–37.
- Domanski, K., Roose, B., Matsui, T., Saliba, M., Turren-Cruz, S.H., Correa-Baena, J.P., Carmona, C.R., Richardson, G., Foster, J.M., Angelis, F.D., Ball, J.M., Petrozza, A., Mine, N., Nazeeruddin, M.K., Tress, W., Grätzel, M., Steiner, U., Hagfeldt, A., Abate, A., 2017. *Energy Environ. Sci.* 10 (2), 604–613.
- Docampo, P., Ball, J.M., Darwich, M., Eperon, G.E., Snaith, H.J., 2013a. *Nat. Commun.* 4, 1–6.
- Docampo, P., Eperon, G.E., Snaith, H.J., Goriely, A., Burlakov, V.M., 2013b. *Adv. Funct. Mater.* 24, 151–157.
- Domanski, K., Alharbi, E.A., Hagfeldt, A., Gratzel, M., 2018. *Nat. Energy* 3, 61–67.
- Dong, Q., Shi, Y., Zhang, C., Wu, Y., Wang, L., 2017. *Nano Energy* 40, 336–344.
- Dong, J., Zhao, Y., Shi, J., Wei, H., Xiao, J., Xu, X., Luo, J., Xu, J., Li, D., Luo, Y., Meng, Q., 2014. *Chem. Commun.* 50, 13381–13384.
- Dualeh, A., Tetreault, N., Moehl, T., Gao, P., Nazeeruddin, M.K., Grätzel, M., 2014. *Adv. Funct. Mater.* 24, 3250–3258.
- Dupré, O., Niesen, B., Wolf, S.D., Ballif, C., 2018. *J. Phys. Chem. Lett.* 9, 446–458.
- Einstein, A., 1905. *Ann. Phys.* 17 (132), 4.
- Eperon, G.E., Burlakov, V.M., Docampo, P., Goriely, A., Snaith, H.J., 2014a. *Adv. Funct. Mater.* 24, 151–157.
- Eperon, G.E., Leijtens, T., Bush, K.A., Prasanna, R., Green, T., Wang, J.T.W., 2016. *Science* 354 (6314), 861–865.
- Eperon, G.E., Stranks, S.D., Menelaou, C., Johnston, M.B., Herz, L.M., Snaith, H.J., 2014b. *Energy Environ. Sci.* 7, 982–988.
- Frits, C.E., 1883. *Am. J. Sci.* 26, 465–472. <https://doi.org/10.2475/ajs.s3-26.156.465>.
- Fu, Q., Tang, X., Huang, B., Hu, T., Tan, L., Chen, L., Chen, Y., 2018. *Adv. Sci.* 5 (5), 1700387.
- Fujishima, A., Rao, T.N., Tryk, D.A., 2000. *J. Photochem. Photobiol. C* 1, 1–21.
- Gao, L., Spanopoulos, I., Ke, W., Huang, S., Hadar, I., Chen, L., Li, X., Yang, G., Kanatzidis, M.G., 2019. *ACS Energy Lett.* 4, 1763–1769.
- Gee, J.M., 1988. *Solar Cells* 24, 147–155.
- Giordano, F., Abate, A., Baena, J.P.C., Saliba, M., Matsui, T., Im, S.H., Zakeeruddin, S.M., Nazeeruddin, M.K., Hagfeldt, A., Gratzel, M., 2016. *Nat. Commun.* 7, 1–6.
- Goldschmidt, V.M., 1926. *Die Naturwissenschaften* 14, 477–485.
- Gonzalez-Pedro, V., Juarez-Perez, E.J., Arsyad, W.S., Barea, E.M., Fabregat-Santiago, F., Mora-Sero, I., Bisquert, J., 2014. *Nano Lett.* 14 (2), 888–893.
- Green, M.A., Hishikawa, Y., Dunlop, E.D., Levi, D.H., Ebinger, J.H., Ho-Baillie, A.W.Y., 2018. *Solar cell efficiency tables (version 57)* Progress in photovoltaics. Res. Appl. 26 (1), 3–12.
- Green, M.A., Dunlop, E.D., Hohl-Ebinger, J., Yoshita, M., Kopidakis, N., Hao, X., 2020. *Solar cell efficiency tables (version 56)*. Prog. Photovoltaics Res. Appl. 28 (7), 629–638.
- Green, M.A., Dunlop, E.D., Hohl-Ebinger, J., Yoshita, M., Kopidakis, N., Hao, X., 2021. *Solar cell efficiency tables (version 58)*. Prog. Photovoltaics Res. Appl. 29 (7), 657–667.
- Gu, P.Y., Wang, N., Wang, C., Zhou, Y., Long, G., Tian, M., Chen, W., Sun, X.W., Kanatzidis, M.G., Zhang, Q., 2017. *J. Mater. Chem. A* 5, 7339–7344.
- Gubbala, S., Chakrapani, V., Kumar, V., Sunkara, M.K., 2008. *Adv. Funct. Mater.* 18, 2411–2418.
- Gujar, T.P., Unger, T., Schonleber, A., Fried, M., Panzer, F., van Smaalen, S., Kohler, A., Thelakkat, M., 2018. *Phys. Chem. Chem. Phys.* 20(1), 605–614.
- Guo, Y., Shoyama, K., Sato, W., Nakamura, E., 2016. *Adv. Energy Mater.* 6, 1502317. <https://doi.org/10.1002/aenm.201502317>.
- Haider, M., Zhen, C., Wu, T., Liu, G., Cheng, H.M., 2018. *J. Mater. Sci. Technol.* 34, 1474–1480.
- Han, Y., Meyer, S., Dkhissi, Y., Weber, K., Pringle, J.M., Bach, U., Spiccia, L., Cheng, Y.B., 2015. *J. Mater. Chem. A* 3, 8139–8147.
- Hashmi, S.G., Martineau, D., Dar, M.I., Myllymäki, T.T.T., Sarikka, T., Ulla, V., Zakeeruddin, S.M., Grätzel, M., 2017. *J. Mater. Chem. A* 5, 12060–12067.
- Henry, C.H., 1980. *J. Appl. Phys.* 51, 4494.
- Heo, J.H., Han, H.J., Kim, D., Ahn, T.K., Im, S.H., 2015. *Energy Environ. Sci.* 8, 1602–1608.
- Hirasawa, M., Ishihara, T., Goto, T., Uchida, K., Miura, N., 1994. *Phys. B: Condensed Matter* 201, 427–430.
- Holzhey, P., Saliba, M., 2018. *J. Mater. Chem. A* 6, 21794.
- Huang, F., Jiang, L., Pascoe, A.R., Yan, Y., Bach, U., Spiccia, L., Cheng, Y.B., 2016. *Nano Energy* 27, 509–514.
- Hwang, I., Jeong, I., Lee, J., Ko, M.J., Yong, K., 2015. *ACS Appl. Mater. Interfaces* 7, 17330–17336.
- IEC 61215-2, 2016. *IEC Webstore*, rural electrification, solar power, solar panel, photovoltaic, PV, smart city, LVDC, Retrieved in July, 2022.
- Im, J.H., Lee, C.R., Lee, J.W., Park, S.W., Park, N.G., 2011. *Nanoscale* 3 (10), 4088–4093.
- Im, J.H., Jiang, I., Pellet, N., Park, N.G., 2014. *Nat. Nanotechnol.* 9 (11), 927–932.
- Jackson, E.D., 1958. *Transaction Conference on the Use of Solar Energy* (University of Arizona Press, Tucson) 5, 122.
- Jäger, K., Tillmann, P., Katz, E.A., Becker, C., 2021. *Solar RRL* 5 (3), 2000628.
- Jeng, J.Y., Chiang, Y.F., Lee, M.H., Peng, S.R., Guo, T.F., Chen, P., Wen, T.C., 2013. *Adv. Mater.* 25, 3727–3732.
- Jeng, J.Y., Chen, K.C., Chiang, T.Y., Lin, P.Y., Tsai, T.D., Chang, Y.C., Guo, T.F., Chen, P., Wen, T.C., Hsu, Y.J., 2014. *Adv. Mater.* 26, 4107–4113.
- Jiang, Q., Zhao, Y., Zhang, X., Yang, X., Chen, Y., Chu, Z., Ye, Q., Li, X., Yin, Z., You, J., 2019. *Nat. Photonics* 13 (7), 460–466.
- Joshi, P., Zhang, L., Hossain, I., Abbas, H.A., Kottokaran, R., Nehra, S., Dhaka, M., Noack, M., Dalal, V., 2016. *AIP Adv.* 6, 115114.
- Katz, E.A., 2020. *Helv. Chim. Acta* 103 (6), e2000061.
- Ke, W., Fang, G., Liu, Q., Xiong, L., Qin, P., Liu, Q., Tao, H., Wang, J., Lei, H., Li, B., Wan, J., Yang, G., Yan, Y., 2015. *J. Am. Chem. Soc.* 137, 6730–6733.
- Khan, F., Rezgui, B.D., Khan, M.T., Al-Sulaiman, F., 2022. *Renew. Sustain. Energy Rev.* 165, 112553.
- Khan, M.A.K., Urmi, S.S., Ferdous, T.T., Azam, S., Ahim, M.A., 2021. *Superlattices Microstruc.* 156, 106946.
- Khanzada, L.S., Levchuk, I., Hou, Y., Azimi, H., Osvet, A., Ahmad, R., Brandl, M., Herre, P., Distaso, M., Hock, R., Peukert, W., Batentschuk, M., Brabec, C.J., 2016. *Adv. Funct. Mater.* 26, 8300–8306.
- Khenkin, M.V., Anoop, K.M., Visoly-Fisher, I., Galagan, Y., Giacomo, F.D., Patil, B.R., Sherafatipour, G., Turkovic, V., Rubahn, H.G., Madsen, M., Merckx, T., Utterhoeven, G., Bastos, J.P.A., Aerouts, T., Brunetti, F., Lira-Cantu, M., Katz, E.A., 2018. *Energy Environ. Sci.* 11 (4), 739–743.
- Khenkin, M.V., Anoop, K.M., Katz, E.A., Visoly-Fisher, I., 2019. *Energy Environ. Sci.* 12, 550–558.
- Khenkin, M.V., Katz, E.A., Abate, A., Bardizza, G., Berry, J.J., et al., 2020. *Nat. Energy* 5, 35–49.
- Kim, H.B., Choi, H., Jeong, J., Kim, S., Walker, B., Song, S., Kim, J.Y., 2014c. *Nanoscale* 6 (12), 6679–6683.
- Kim, H.S., Im, S.H., Park, N.G., 2014a. *J. Phys. Chem. C* 118 (11), 5615–5625.
- Kim, J., Kim, G., Kim, T.K., Kwon, S., Back, H., Lee, J., Lee, S.H., Kang, H., Lee, K., 2014b. *J. Mater. Chem. A* 2, 17291–17296.
- Kim, B.J., Kim, D.H., Lee, Y.Y., Shin, H.W., Han, G.S., Hong, J.S., Mahmood, K., Ahn, T., Koo, Y.C., Hong, K.S., Park, N.G., Lee, S., Jung, H.S., 2015a. *Energy Environ. Sci.* 8, 916–921.
- Kim, H.S., Lee, C.R., Im, J.H., Lee, K.B., Moehl, T., Marchioro, A., Moon, S.J., Baker, R.H., Yum, J.H., Moser, J.E., Gratzel, M., Park, N.G., 2012. *Sci. Rep.* 2 (1), 1–7. <https://doi.org/10.1038/srep00591>.

- Kim, J.H., Liang, P.W., Williams, S.T., Cho, N., Chueh, C.C., Glaz, M.S., Gingerand, D.S., Jen, A.K.Y., 2015b. *Adv. Mater.* 27, 695–701.
- Kim, H.S., Seo, J.Y., Park, N.G., 2016. *Chem.-Sustain.-Chem. Mater.* 9 (18), 2528–2540. <https://doi.org/10.1002/cssc.201600915>.
- King, R.R., Law, D.C., Edmondson, K.M., Fetzer, C.M., Sherif, R.A., Kinsey, G.S., Krut, D.D., Cotal, H.L., Karam, N.H., 2006. In: Proceedings of the IEEE 4th World Conference on Photovoltaic Energy Conversion, Waikoloa, HI, USA, 760–763.
- King, R.R., Law, D.C., Edmondson, K.M., Fetzer, C.M., Kinsey, G.S., Yoon, H., Sherif, R.A., Karam, N.H., 2007. *Appl. Phys. Lett.* 90, 183516.
- Kojima, A., Teshima, K., Shirai, Y., Miyasaka, T., 2009. *J. Am. Chem. Soc.* 131 (17), 6050–6051.
- Kumari, N., Gohel, J.V., Patel, S.R., 2018b. *Mater. Sci. Semiconductor Process.* 75, 149–156.
- Kumari, N., Patel, S.R., Gohel, J.V., 2018c. *J. Mater. Sci.: Mater. Electron.* 29 (21), 18144–18150.
- Kumari, N., Patel, S.R., Gohel, J.V., 2018a. *Rev. Adv. Mater. Sci.* 53, 161–186.
- Kumari, N., Patel, S.R., Gohel, J.V., 2019. *Optik* 176, 262–277.
- Kundu, S., Kelly, T.L., 2018. *Mater. Chem. Front.* 2 (1), 81–89.
- Lee, J.W., Park, N.G., 2020. *Adv. Energy Mater.* 10 (1), 1903249.
- Lee, M.M., Teuscher, J., Miyasaka, T., Murakami, T.N., Snaith, H.J., 2012. *Science* 338, 643–647.
- Leguy, A.M.A., Hu, Y., Quiles, M.C., Alonso, M.I., Weber, O.J., Azarhoosh, P., Schilfhaar, M.V., Weller, M.T., Bein, T., Nelson, J., Docampo, P., Barnes, P.R.F., 2015. *Chem. Mater.* 27, 3397–3407.
- Leijten, T., Eperon, G.E., Pathak, S., Abate, A., Lee, M.M., Snaith, H.J., 2013. *Nat. Commun.* 4 (1), 1–8.
- Letcher, T.M., Fthenakis, V.M., 2018. A comprehensive guide to solar energy systems with special focus on photovoltaic systems. Elsevier Academic Press, Chapter 11, 233–247.
- Li, X., Bi, D., Yi, C., Décupet, J.D., Luo, J., Zakeeruddin, S.M., Hagfeldt, A., Gratzel, M., 2016. *Science* 353 (6294), 58–62.
- Li, C., Soh, K.C.K., Wu, P., 2004. *J. Alloys Compd.* 372, 40–48.
- Li, C., Lu, X., Ding, W., Feng, L., Gao, Y., Guo, Z., 2008. *Acta Crystallographica Section B* 64, 702–707.
- Li, T., Pan, Y., Wang, Z., Xia, Y., Chen, Y., Huang, W., 2017. *J. Mater. Chem. A* 5, 12602–12652.
- Li, Y., Zhu, J., Huang, Y., Liu, F., Lv, M., Chen, S., Hu, L., Tang, J., Yao, J., Dai, S., 2015. *RSC Adv.* 5, 28424–28429.
- Lin, L., Jones, T.W., Yang, T.C.J., Duffy, N.W., Li, J., Zhao, L., Chi, B., Wang, X., Wilson, G.J., 2021. *Adv. Funct. Mater.* 31 (5), 2008300.
- Liu, C., Fan, J., Li, H., Zhang, C., Mai, Y., 2016. *Sci. Rep.* 6, 1–8.
- Liu, M., Johnston, M.B., Snaith, H.J., 2013. *Nature* 501, 395–398.
- Liu, D., Kelly, T.L., 2014. *Nat. Photonics* 8, 133–138.
- Ludowise, M.J., 1986. U.S. patent 4575576.
- Luo, D., Li, X., Dumont, A., Yu, H., Lu, Z.H., 2021. *Adv. Mater.* 33 (30), 2006004.
- Luo, Q., Zhang, Y., Liu, C., Li, J., Wang, N., Lin, H., 2015. *J. Mater. Chem. A* 3, 15996–16004.
- Mahmood, K., Swain, B.S., Amassian, A., 2014. *Nanoscale* 6, 14674–14678.
- Ma, S., Yuan, G., Zhang, Y., Yang, N., Li, Y., Chen, Q., 2022. *Energy Environ. Sci.* 15, 13–55.
- Malinauskas, T., Luksiene, D.T., Sens, R., Daskeviciene, M., Send, R., Wonneberger, H., Jankauskas, V., Bruder, I., Getautis, V., 2015. *ACS Appl. Mater. Interfaces* 7, 11107–11116.
- Maniarasu, S., Korukonda, T.B., Manjunath, V., Ramasamy, E., Ramesh, M., Veerappan, G., 2018. *Renew. Sustain. Energy Rev.* 82, 845–857.
- Manor, A., Katz, E.A., Tromholt, T., Krebs, F.C., 2011. *Adv. Energy Mater.* 1, 836.
- Meulenkamp, E.A., 1999. *J. Phys. Chem. B* 103, 7831–7838.
- Minemoto, T., Murata, M., 2014. *J. Appl. Phys.* 116 (5), 054505.
- Misra, R.K., Aharon, S., Li, B., Mogilyansky, D., Visoly-Fisher, I., Etgar, L., Katz, E.A., 2015. *J. Phys. Chem. Lett.* 6 (3), 326–330.
- Mitzi, D.B., Chondroudis, K., Kagan, C.R., 1999. *Inorg. Chem.* 38, 6246–6256.
- Mitzi, D.B., Chondroudis, K., Kagan, C.R., 2001. *IBM J. Res. Dev.* 45, 29–45.
- Naghadeh, S.B., Luo, B., Abdelmageed, G., Pu, Y.C., Zhang, C., Zhang, J.Z., 2018. *J. Phys. Chem. C* 122, 15799–15818.
- Nair, S., Patel, S.B., Gohel, J.V., 2020. *Mater. Today Energy* 17, 100449.
- Nelson, J., 2002. *The Physics of Solar Cells*. Imperial College Press.
- Nia, N.Y., Matteocci, F., Cina, L., Carlo, A.D., 2017. *Chem. Sustain. Energy Mater.* 10, 3854–3860. <https://doi.org/10.1002/cssc.201700635>.
- Niu, G., Li, W., Meng, F., Wang, L., Dong, H., Qiu, Y., 2014. *J. Mater. Chem. A* 2, 705–710.
- Niu, G., Guo, X., Wang, L., 2015. *J. Mater. Chem. A* 3, 8970–8980.
- NREL Best Research-Cell Efficiency Chart, 2022. <https://www.nrel.gov/pv/assets/pdfs/best-research-cell-efficiencies-rev220630.pdf>, Retrieved in July, 2022.
- Noh, J.H., Im, S.H., Heo, J.H., Mandal, T.N., 2013a. *Nano Lett.* 13, 1764–1769.
- Noh, J.H., Jeon, N.J., Choi, Y.C., Nazeeruddin, M.K., Gratzel, M., Seok, S. II, 2013b. *J. Mater. Chem. A* 1, 11842–11847.
- Olson, J.M., Kurtz, S.R., Kibbler, A.E., Faine, P., 1990. *Appl. Phys. Lett.* 56, 623–625.
- Oxford PV perovskite solar cell achieves 28% efficiency, 2018. <https://www.oxfordpv.com/news/oxford-pv-perovskite-solar-cell-achieves-28-efficiency>, Retrieved in July, 2022.
- Park, N.G., Graetzel, M., Miyasaka, T., 2016. *Cham. Springer, Switzerland*.
- Patel, S.B., Patel, A.H., Gohel, J.V., 2018. *Cryst. Eng. Commun.* 20, 7677–7687.
- Peleg, R., 2018. Microquanta Reaches 17.9% Efficiency for Perovskite Solar Mini-Module, Perovskite-Info, <https://www.perovskite-info.com/microquanta-reaches-179-efficiency-perovskite-solar-mini-module>, Retrieved in July, 2022.
- Pellet, N., Gao, P., Gregori, G., Yang, T.Y., Nazeeruddin, M.K., Maier, J., Gratzel, M., 2014. *Angew. Chem. Int. Ed.* 53, 3151–3157.
- Poglitsch, A., Weber, D., 1987. *J. Chem. Phys.* 87, 6373.
- Poorkazem, K., Kelly, T.L., 2017. *ACS Appl. Energy Mater.* 1 (1), 181–190.
- Prete, M., Khenkin, M.V., Glowienka, D., Patil, B.R., Lissau, J.S., Dogan, I., Hansen, J.L., Leibnér, T., Fiutowski, J., Rubahn, H.G., Julsgaard, B., Balling, P., Turkovic, V., Galagan, Y., Katz, E.A., Madsen, M., 2021. *ACS Appl. Energy Mater.* 4, 6562–6573.
- Qiu, Q., Liu, H., Qin, Y., Ren, C., Song, J., 2020. *J. Mater. Sci.* 55 (28), 13881–13891.
- Rombach, F.M., Haque, S.A., Macdonald, T.J., 2021. *Energy Environ. Sci.* 14, 5161–5190. DOI: <https://doi.org/10.1039/D1EE02095A>.
- Rose, G., 1839. *Poggendorffs Annalen der Physik und Chemie* 551–573.
- Ro, P., Sinha, N.K., Tiwari, S., Khare, A., 2020. *Sol. Energy* 198, 665–688.
- Saliba, M., Matsui, T., Seo, J.Y., Domanski, K., Baena, J.P.C., Nazeeruddin, M.K., Zakeeruddin, S.M., Tress, W., Abate, A., Hagfeldt, A., Gratzel, M., 2016. *Energy Environ. Sci.* 9, 1898–1997.
- Schnabel, M., Schulte-Huxel, H., Rienäcker, M., Warren, E.L., Ndione, P.F., Nemeth, B., Klein, T.R., VanHest, M.F.A.M., Geisz, J.F., Peibst, R., Stradins, P., Tamboli, A.C., 2020. *Sustain. Energy Fuels* 4, 549–558.
- Shao, S., Liu, J., Portale, G., Fang, H.H., Blake, G.R., Brink, G.H.T., Koster, L.J.A., Loi, M.A., 2018. *Adv. Energy Mater.* 8 (4), 1702019.
- Sheng, R., Baillie, A.H., Huang, S., Chen, S., Wen, X., Hao, X., Green, M.A., 2015. *J. Phys. Chem. C* 119, 3545–3549.
- Siempelkamp, B.D., Kelly, T.L., Yang, J., Mosconi, E., Angelis, F.D., 2015. *Chem. Mater.* 27, 4229–4236.
- Smith, W., 1873. *J. Soc. Telegraph Eng.* 2, 31–33.
- Snaith, H.J., 2013. *J. Phys. Chem. Lett.* 4, 3623–3630.
- Solaronix Achieves Major Breakthrough Toward Perovskite Solar Cell Industrialization, 2016. <https://www.solaronix.com/news/solaronix-achieves-major-breakthrough-toward-perovskite-solar-cell-industrialization>, Retrieved in July, 2022.
- Son, D.Y., Im, J.H., Kim, H.S., Park, N.G., 2014. *J. Phys. Chem. C* 118, 16567–16573. DOI: <https://doi.org/10.1021/jp412407j>.
- Song, J., Liu, L., Wang, X.F., Chen, G., Tian, W., Miyasaka, T., 2017. *J. Mater. Chem. A* 5, 13439–13447.
- Song, Z., Watthage, S.C., Phillips, A.B., Heben, M.J., 2016. *J. Photonics Energy* 6 (2), 022001.
- Stoumpos, C.C., Malliakas, C.D., Kanatzidis, M.G., 2013. *Inorg. Chem.* 52, 9019–9038.
- Sun, W., Ye, S., Rao, H., Li, Y., Liu, Z., Xiao, L., Chen, Z., Bian, Z., Huang, C., 2016. *Nanoscale* 8, 15954–15960.
- Sutton, R.J., Eperon, G.E., Miranda, L., Parrott, E.S., Kamino, B.A., Patel, J.B., Hörrantner, M.T., Johnston, M.B., Haghhighirad, A.A., Moore, D.T., Snaith, H.J., 2016. *Adv. Energy Mater.* 6 (8), 1502458.
- Takamoto, T., Ikeda, E., Kurita, H., Ohmori, M., 1997. *Appl. Phys. Lett.* 70, 381–383.
- Tang, J., Jiao, D., Zhang, L., Zhang, X., Xu, X., Yao, C., Wu, J., Lan, Z., 2018. *Sol. Energy* 161, 100–108.
- Tao, S.X., Cao, X., Bobbert, P.A., 2017. *Sci. Rep.* 7 (1), 1–9.
- The History of Solar Energy, 2013. <https://energyinformative.org/the-history-of-solar-energy-timeline/>, Retrieved in July, 2022.
- Thind, A.S., Kavadiya, S., Kouhnnavard, M., Wheelus, R., Cho, S.B., Lin, L.Y., Kacica, C., Mulmudi, H., Unocic, K.A., Borisevich, A.Y., Pilania, G., Biswas, P., Mishra, R., 2019. *Chem. Mater.* 31 (13), 4769–4778.
- Todorov, T., Gershon, T., Gunawan, O., Sturdevant, C., Guha, S., 2014. *Appl. Phys. Lett.* 105, 173902.
- Travis, W., Glover, E.N.K., Bronstein, H., Scanlon, D.O., Palgrave, R.G., 2016. *Chem. Sci.* 7, 4548–4556.
- Tress, W., Marinova, N., Moehl, T., Zakeeruddin, S.M., Nazeeruddin, M.K., Gratzel, M., 2015. *Energy Environ. Sci.* 8, 995–1004.
- Tseng, Z.L., Chiang, C.H., Wu, C.G., 2015. *Sci. Rep.* 5, 1–10.
- Umari, P., Mosconi, E., De Angelis, F., 2014. *Sci. Rep.* 4 (1), 1–7.
- Valverde-Chavez, D.A., Ponseca Jr., C.S., Stoumpos, C.C., Yartsev, A., Kanatzidis, M.G., Sundstrom, V., Cooke, D.G., 2015. *Energy Environ. Sci.* 8 (12), 3700–3707.
- Wali, Q., Iftekhar, F.J., Khan, M.E., Ullah, A., Iqbal, Y., Jose, R., 2020. *Org. Electron.* 78, 10590.
- Wang, J., Amini, A., Liu, C., Xu, B., Li, D., Yang, S., Liu, H., Kong, W., Hu, M., Li, W., Miao, J., Chen, S., Wang, W., Cheng, C., 2019. *ACS Nano* 13 (2), 1625–1634.
- Wang, Q., Shao, Y., Dong, Q., Xiao, Z., Yuan, Y., Huang, J., 2014. *Energy Environ. Sci.* 7, 2359–2365. DOI: <https://doi.org/10.1039/C4EE00233D>.
- Wang, D., Wright, M., Elumalai, N.K., Uddin, A., 2016a. *Sol. Energy Mater. Sol. Cells* 147, 255–275.
- Wang, H., Yu, Z., Jiang, X., Li, J., Cai, B., Yang, X., Sun, L., 2017. *Energy Technol.* 5, 1836–1843.
- Wang, C., Zhao, D., Grice, C.R., Liao, W., Yu, Y., Cimaroli, A., Shrestha, N., Roland, P.J., Chen, J., Yu, Z., Liu, P., Cheng, N., Ellingson, R.J., Zhao, X., Yan, Y., 2016b. *J. Mater. Chem. A* 4, 12080–12087.
- Warren, E.L., McMahan, W.E., Rienäcker, M., VanSant, K.T., Whitehead, R.C., Peibst, R., Tamboli, A.C., 2020. *ACS Energy Lett.* 5, 1233–1242.
- Werner, J., Niesen, B., Ballif, C., 2018. *Adv. Mater. Interfaces* 5 (1), 1700731.
- Wu, W.Q., Liu, Y., Huang, J., Fang, Y., Gruverman, A., Yang, Z., Li, T., Deng, Y., Lu, H., Shao, Y., Wang, Q., Tang, S., 2018. *Nat. Commun.* 9, 1–8.
- Wu, T., Qin, Z., Wang, Y., Wu, Y., Chen, W., Zhang, S., Cai, M., Dai, S., Zhang, J., Liu, J., Zhou, Z., Liu, X., Segawa, H., Tan, H., Tang, Q., Fang, J., Li, Y., Ding, L., Ning, Z., Qi, Y., Zhang, Y., Han, L., 2021. *Nano-Micro Lett.* 13 (1), 1–18.
- Wu, Q., Xue, C., Li, Y., Zhou, P., Liu, W., Zhu, J., Dai, S., Zhu, C., Yang, S., 2015. *ACS Appl. Mater. Interfaces* 7, 28466–28473.
- Xie, F., Chen, C.C., Wu, Y., Li, X., Cai, M., Liu, X., Yang, X., Han, L., 2017. *Energy Environ. Sci.* 10, 1942–1949.

- Xing, G., Mathews, N., Lim, S.S., Yantara, N., Sabba, D., Gratzel, M., Mhaisalkar, S., Sum, T.C., 2014. *Nat. Mater.* 13 (5), 476–480.
- Xing, G., Mathews, N., Sun, S., Lim, S.S., Lam, Y.M., Gratzel, M., Mhaisalkar, S., Sum, T.C., 2013. *Science* 342 (6156), 344–347.
- Xu, B., Bi, D., Hua, Y., Liu, P., Cheng, M., Gratzel, M., Kloo, L., Hagfeldt, A., Sun, L., 2016a. *Energy Environ. Sci.* 9, 873–877.
- Xu, L., Dai, Y., Zhang, H., Huang, W., 2016b. *RSC Adv.* 6, 48449–48454.
- Xu, X., Zhang, H., Shi, J., Dong, J., Luo, Y., Li, D., Meng, Q., 2015. *J. Mater. Chem. A* 3, 19288–19293.
- Yamaguchi, M., Dimroth, F., Geisz, J.F., Ekins-Daukes, N.J., 2021. *J. Appl. Phys.* 129, 240901.
- Yang, W.S., Noh, J.H., Jeon, N.J., Kim, Y.C., Ryu, S., Seo, J., Seok, S.I., 2015. *Science* 348 (6240), 1234–1237.
- Yang, W.S., Park, B.W., Jung, E.H., Jeon, N.J., Kim, Y.C., Lee, D.U., Shin, S.S., Seo, J., Kim, E.K., Noh, J.H., Seok, S.I., 2017. *Science* 356, 1376–1379.
- Yang, D., Yang, R., Wang, K., Wu, C., Zhu, X., Feng, J., Ren, X., Fang, G., Priya, S., Liu, S., 2018. *Nat. Commun.* 9.
- Yang, D., Yang, R., Priya, S., Liu, S., 2019. *Angew. Chem.* 58 (14), 4466–4483.
- Yu, Z., Sun, L., 2015. *Adv. Energy Mater.* 5 (12), 1500213.
- Zhang, Y., Kim, S.G., Lee, D., Shin, H., Park, N.G., 2019. *Energy Environ. Sci.* 12, 308–321.
- Zhang, R., Liu, D., Wang, Y., Zhang, T., Gu, X., Zhang, P., Wu, J., Chen, Z.D., Zhao, Y., Li, S., 2018. *Electrochim. Acta* 265, 98–106.
- Zhao, Y., Wei, J., Li, H., Yan, Y., Zhou, W., Yu, D., Zhao, Q., 2016. *Nat. Commun.* 7, 10228.
- Zuo, C., Scully, A.D., Vak, D., Tan, W., Jiao, X., McNeill, C.R., Angmo, D., Ding, L., Gao, M., 2019. *Adv. Energy Mater.* 9, 1–9.